

Multifunctional layered black phosphorene-based nanoplatform for disease diagnosis and treatment: a review

Xiazi HUANG^{1,2†}, Yingying ZHOU^{1,2†}, Chi Man WOO^{1,2}, Yue PAN³, Liming NIE⁴, Puxiang LAI (✉)^{1,2}

¹ Department of Biomedical Engineering, Hong Kong Polytechnic University, Hong Kong, China

² Hong Kong Polytechnic University Shenzhen Research Institute, Shenzhen 518057, China

³ Guangdong Provincial Key Laboratory of Malignant Tumor Epigenetics and Gene Regulation, Medical Research Center, Sun Yat-Sen Memorial Hospital, Sun Yat-Sen University, Guangzhou 510120, China

⁴ State Key Laboratory of Molecular Vaccinology and Molecular Diagnosis & Center for Molecular Imaging and Translational Medicine, School of Public Health, Xiamen University, Xiamen 361102, China

© Higher Education Press 2020

Abstract As an outstanding two-dimensional material, black phosphorene, has attracted significant attention in the biomedicine field due to its large surface area, strong optical absorption, distinct bioactivity, excellent biocompatibility, and high biodegradability. In this review, the preparation and properties of black phosphorene are summarized first. Thereafter, black phosphorene-based multifunctional platforms employed for the diagnosis and treatment of diseases, including cancer, bone injuries, brain diseases, progressive oxidative diseases, and kidney injury, are reviewed in detail. This review provides a better understanding of the exciting properties of black phosphorene, such as its high drug-loading efficiency, photo-thermal conversion capability, high ¹O₂ generation efficiency, and high electrical conductivity, as well as how these properties can be exploited in biomedicine. Finally, the research perspectives of black phosphorene are discussed.

Keywords black phosphorus (BP), delivery nanoplatform, bioimaging, cancer therapy, bone regeneration

1 Introduction

In recent years, two-dimensional (2D) materials have attracted significant interest due to their optical, catalytic, and tunable electronic and electrochemical properties [1–5]. For example, since graphene was successfully

synthesized in 2004, it has become one of the most extensively studied 2D materials [6,7]. Graphene has excellent properties beneficial for optoelectronic and electronic applications; it also has a large surface area ideally suitable for drug delivery in biomedicine [8,9]. The success of graphene has inspired the development of many other 2D materials, such as silicene [10] transition-metal dichalcogenides (MoSe₂, WSe₂ and MoS₂), transition-metal oxides [11–13], and black phosphorus (BP) [14,15]. Notably, BP distinguishes itself from all other 2D materials, as it exhibits exclusive properties relevant to diverse fields, particularly biomedicine [16].

For instance, BP exhibits excellent adsorption capacity due to its unique structure. Single-layer BP is composed of one P atom bonded to two neighboring intraplanar P atoms and another P atom in an adjacent interplane via p-orbitals (Figs. 1(a) and 1(b)) [17]. Each BP layer is held together by relatively weak van der Waals (vdWs) forces; thus, layered BP can be achieved by bulk BP exfoliation [18,19]. Furthermore, the puckered honeycomb lattice-layered structure of BP provides a large surface area for improved drug-loading efficiency [20]. In addition to the non-covalent bonding with drugs, fluorescent molecules, bioactive molecules, and metal atoms, positively charged particles can be tightly bonded to the negatively charged BP through electrostatic interactions [21–24]. These unique properties make layered BP a versatile platform for extensive biomedical applications, such as targeted drug delivery, biomolecule detection, and cell imaging.

Moreover, the strong interactions between electromagnetic waves (such as visible and near-infrared (NIR) light) and BP can be effectively regulated in a layer-dependent manner from the ultraviolet to the NIR regions, due to the tunable bandgap of BP (0.3–2.0 eV). This appealing

Received August 19, 2020; accepted October 1, 2020

E-mail: puxiang.lai@polyu.edu.hk

[†] Equal contribution

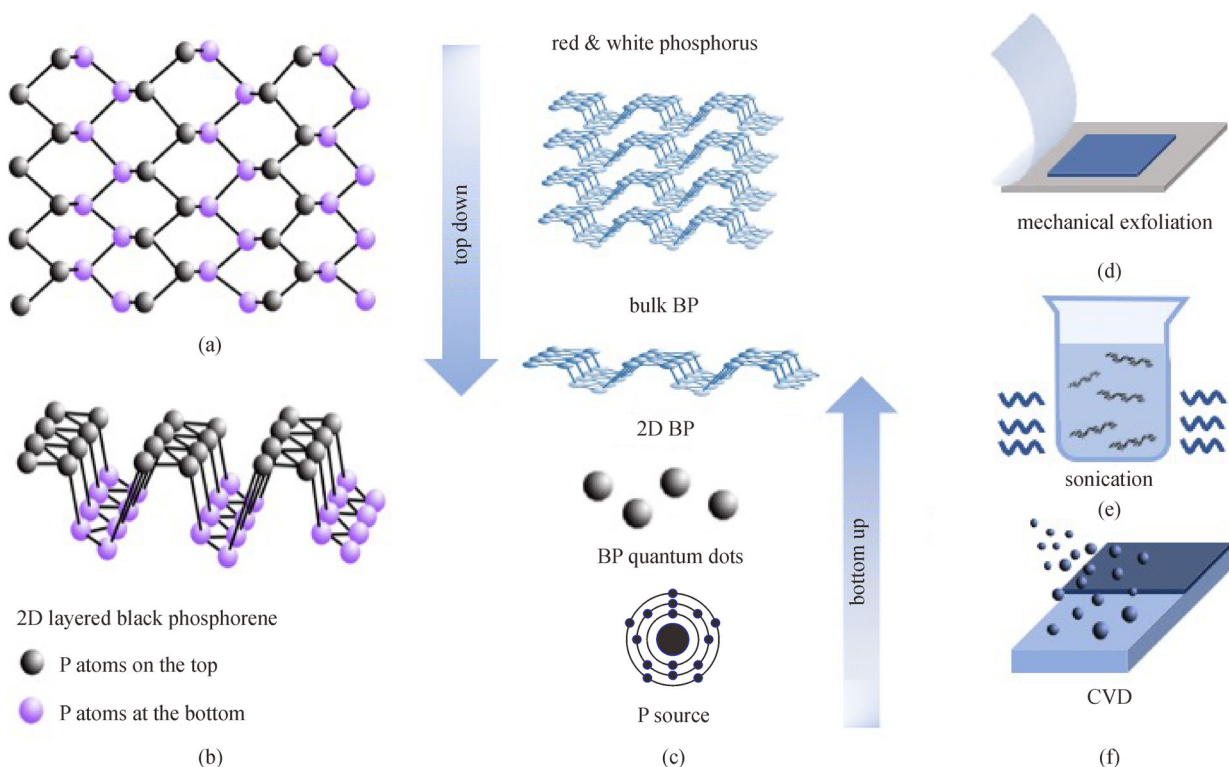


Fig. 1 Schematic illustration of the atomic structure of 2D BP. (a) Top view. (b) 3D view. Reproduced from Ref. [17]. (c) Schematic illustration of the 2D layered-BP preparation methods. (d) Schematic illustration of mechanical exfoliation. (e) Schematic illustration of liquid-phase exfoliation. (f) Schematic illustration of the CVD method

property endows BP with promising optical potentials, such as photoredox capability and a large extinction coefficient [16]. Such a layer-dependent band gap property is a prerequisite for various applications in photonic devices and electronics, such as biosensors [25–28], which can be used to detect target microRNA in concentrations as low as 0.3 pmol/L [29]. Moreover, BP nanosheets (BPNSs) can be applied as photoacoustic (PA) contrast and photothermal agents for noninvasive PA imaging [30] and photothermal therapy (PTT), respectively, because of their large extinction coefficients and high photothermal conversion efficiency [31,32]. In particular, BPNSs can generate toxic single oxygen ($^1\text{O}_2$) when exposed to external laser irradiations; therefore, they can act as photosensitizers in photodynamic therapy (PDT) [33,34].

Finally, compared with other popular 2D nanomaterials such as graphene, layered BP has negligible cytotoxicity and excellent biodegradability, which is ideal for *in vivo* applications [35]. The high biodegradability of BP *in vivo* makes it safe for use in the human body, particularly because its biodegradation produces nontoxic intermediate products, such as phosphate, phosphite, and other P_xO_y products [36,37].

Therefore, BPNSs could be an almighty nanoplatform for multidisciplinary biomedical applications [14,38,39]. In this review, we summarize the synthesis methods of BPNSs and discuss their properties; we also discuss

BPNS-based multifunctional nanomaterials and their applications for disease diagnosis and therapy in detail. Last, future research directions and potential applications are envisioned.

2 Preparation of layered BP

Various methods for preparing layered BP have been reported, which can be categorized into “top-down” and “bottom-up” approaches (Fig. 1) [40–42]. The top-down approach usually involves exfoliating the bulk material into single or several layers of nanosheets by driving forces, such as mechanical exfoliation and liquid exfoliation (Figs. 1(d) and 1(e)). The bottom-up approach involves preparing nanomaterials directly from specific precursors by chemical reactions, such as chemical vapor deposition (CVD) (Fig. 1(f)) [43]. These methods are summarized in Table 1.

2.1 Preparation of BP bulk crystal

The preparation of BP bulk crystal is a prerequisite for the “top-down” preparation approach for layered BP. In 1914, Bridgeman first synthesized BP bulk crystals using white P at a temperature of 200°C and pressure of 1.2 GPa for 5–30 min [44]. Red phosphorus (RP) has also been used to

Table 1 Summary of the popular synthesis methods

synthesis method		description	advantages	disadvantages
top-down	mechanical exfoliation	making BP layers flake off and thin from BP bulk crystal by repeatedly bonding/separating with the help of adhesive tapes or plasma etching	<ul style="list-style-type: none"> • high quality BPNSs 	<ul style="list-style-type: none"> • not suitable for large-scale production of BPNSs • hard to control the thickness and size of BPNSs
	liquid exfoliation	BP bulk crystal is immersed into solvents and the ions weaken and break the interlayer attractions between BP layers under sonication	<ul style="list-style-type: none"> • large-scale production • diverse BP nanostructures (e.g., BPQDs and BPNSs) <ul style="list-style-type: none"> • controllable size and thickness of final product • low cost 	<ul style="list-style-type: none"> • hard to produce large area phosphorene • lower purity
bottom-up	chemical vapor deposition (CVD)	forming BP thin films by doping phosphorus atoms in the vacuum	<ul style="list-style-type: none"> • suitable for large area BPNSs production 	<ul style="list-style-type: none"> • high cost • produce by-products

produce BP at high pressure and low cost [45,46]. Later, some improved methods (e.g., catalysis, recrystallization, and flux methods) were used to prepare BP to achieve relatively stable formation, enhanced quality, and a simple process, although these methods had drawbacks, including high toxicity and many by-products [47–49]. Recently, some new methods were introduced to further simplify the process and increase the yield [50–52]. For example, in 2014, Köpf et al. screened the additives in the traditional process of preparing BP from RP and found that removing Au from the reactants can significantly reduce the number of by-products [50].

2.2 Mechanical exfoliation of BP

Generally, mechanical exfoliation and liquid-phase stripping are the most used techniques in BPNS synthesis. Mechanical exfoliation, also known as “peeling,” has been widely applied [53]. BP crystals are composed of vertically overlaid layers under the weak vdWs forces; this layered structure can be micromechanically cleaved to achieve atom-thick BP layers [54,55]. Although large-scale production of BPNSs is still in the preliminary stage, mechanical cleavage is still one of the most effective and commercially available methods for producing small-scale and high-quality BPNSs [56]. The principle of this method is to make BP layers flake off and thin by repeated bonding/separation using adhesive tapes. Thereafter, BP is usually purified with methanol, acetone, and isopropanol to remove the tape residues after transferring onto the SiO₂/Si substrate. The residual solvent is removed by a 180°C postbake process [57,58]. Note that preparing layered BP on SiO₂/Si substrates requires optimal environmental conditions, and the yield is extremely low because of the weak adhesive force. Later, Guan et al. found that the existence of an Ag or Au thin layer on the SiO₂/Si substrates can significantly increase the yield of layered BP [59]. Moreover, by switching to a viscoelastic polydimethylsiloxane substrate, the exfoliation process can be optimized to have increased yield and less contamination from the tape [19]. Nevertheless, this mechanical exfolia-

tion method is not suitable for mass production and can only be used in the laboratory. Another drawback is that the thickness and size of the resultant sheets cannot be systematically controlled. In 2014, Lu et al. first proposed the combination of the mechanical cleavage method with a highly controllable Ar⁺ plasma thinning process to thin down the phosphorene to homogeneous mono-layered phosphorene [60]. However, the thinner the BP, the more unstable it is; as such, it can easily be oxidized during the plasma thinning process, which makes the product uncontrollable. In 2016, Pei et al. used a new method to refine the thick-exfoliated phosphorene flakes layer by layer through oxygen plasma etching; subsequently, they passivated them with Al₂O₃ to produce a controlled and high-quality phosphorene with a designed number of air-stable layers [61].

2.3 Liquid exfoliation of BP

Liquid-phase stripping methods are auspicious for obtaining a large quantity of exfoliated phosphorene nanosheets in various sizes [62,63]. A typical protocol starts with the immersion of a BP bulk crystal in diverse solvents (e.g., water, alcohols, ketones, chloro-organic solvents, cumyl hydroperoxide, and pyrrolidones) to permit the ions to embed and expand the distance between adjacent BP layers [64,65]. The interlayer vdWs attraction breaks down, and the process is accelerated under sonication. Polar and aprotic solvents, such as *N,N*-dimethylformamide (DMF) and dimethyl sulfoxide (DMSO), could be adopted to prepare crystal BPNSs with a controllable thickness. The thickness of > 20% of the exfoliated nanosheets in DMF is < 5 nm, whereas the thickness in DMSO is between 15 and 20 nm [66]. Woomer et al. surveyed and compared the ability of 18 solvents for BP exfoliation [67]. An average concentration of 0.11 ± 0.02 mg/mL in benzonitrile was suggested to be the best solvent. In addition, they demonstrated that one essential condition for preparing phosphorene is that it must be sonicated and manipulated under an inert atmosphere. In 2015, a simple and scalable approach involving the combination of shear mixing and

bath sonication was first used, and it yielded a highly concentrated suspension of few-layered BP [67]. Liquid exfoliation permits the large-scale production of diverse BP nanostructures, such as quantum dots and nanosheets. Such a low cost and simple method allows for applications in solar cells, printable electronics, sensing, phototherapy, and bioimaging [65].

Further, the use of plasma in liquid exfoliation should be discussed. Plasma is a partly ionized gas composed of a variety of active substances, such as high-energy electrons, free radicals, ions, photons, and excited metastable states, and it is used in deposition, surface etching, and material modifications [68,69]. In nanomaterial preparation, the plasma–liquid phase interaction is appealing because a series of reactions can be initiated by the active materials transferred in the plasma–liquid phase [70,71]. In a recent study, plasma–liquid exfoliation was used to prepare layered P, achieving an efficiency of 63% at a concentration of $\sim 300 \mu\text{g/mL}$ [72]. During exfoliation, due to the strong interaction between the active species in the solution and plasma, the DMF decomposes into cationic species. These cationic species (e.g., $\text{C}_2\text{H}_8\text{N}^+$, $\text{C}_3\text{H}_8\text{N}^+$, $\text{C}_2\text{H}_6\text{N}^+$, H^+ , and $\text{C}_2\text{H}_4\text{N}^+$) migrate to the cathodic BP bulk crystal under an electric field and insert themselves into the layered space. Afterward, they accept electrons and form gases (e.g., H_2 , $\text{C}_2\text{H}_7\text{N}$, and $\text{C}_3\text{H}_9\text{N}$) to expand the space in the BP crystal, facilitating the exfoliation process. Compared with traditional liquid stripping, plasma-based liquid exfoliation is more effective because it can produce uniform few-layered P with thicknesses $< 10 \text{ nm}$ rapidly (in 5 min). Comparably, over 10 h is needed in traditional liquid stripping. In addition, plasma–

liquid exfoliation is more suitable for large-scale production with a low cost [73].

2.4 Direct growth of layered-BP thin films

The aforementioned methods have shown promising progress thus far. However, they experience challenges regarding the preparation of large-area phosphorene, which is amenable to the device fabrication process. In this regard, a wafer-scale synthesis method via CVD has been developed for large-area graphene fabrication, which is a breakthrough for large-area layered-BP production [74,75]. In 2015, Li et al. vaporized RP powder on a flexible polyester substrate and synthesized large-area BPNSs (diameters of up to 4 mm) with a thickness of $\sim 40 \text{ nm}$ at room temperature. Transistors incorporating such thin BPNSs deliver a field-effect mobility of $\sim 0.5 \text{ cm}^2/(\text{V}\cdot\text{s})$ [76]. In 2016, Smith et al. mass-produced BP thin films with large areas (above $100 \mu\text{m}^2$) and tens of nanometers in thickness directly on a silicon substrate [77]. However, the crystalline size and mobility of the converted BP were still limited. In 2018, Li et al. synthesized highly crystalline BPNSs on sapphire substrates by converting RP to BP at a pressure of 1.5 GPa and temperature of 700°C . The crystal domain size of the prepared polycrystalline BPNSs could reach as high as $70 \mu\text{m}$ with an average thickness of 50 nm . The field-effect mobility of the prepared BPNS is $\sim 160 \text{ cm}^2/(\text{V}\cdot\text{s})$ along the armchair direction at room temperature; however, it reaches $\sim 200 \text{ cm}^2/(\text{V}\cdot\text{s})$ at 90 K, assuring its performance in the electronic system [78]. Their work is a vital step toward achieving high-quality, large-scale BP circuits and devices in the future.

Table 2 Biomedical applications of layered black phosphorus-based platforms in disease diagnosis and treatment

material	application	disease	highlight of the research	Ref.
TiL ₄ @BPQDs	photoacoustic imaging (PAI)	MCF-7 tumor	It demonstrates that BP-based PA agents are stable and can be used for efficient bioimaging of cancer; the performance is superior to that of gold nanoparticles (AuNPs).	[30]
BP-DEX/PEI-FA	PAI and photothermal therapy (PTT)	BP-DEX/PEI-FA	The biocompatible and water-soluble BP nanoparticles exhibit high photothermal conversion efficacy for PAI and photothermal therapy of cancer.	[79]
BP@lipid-PEG	PAI/NIR-II optical imaging		It first reports that the BPNSs modified with cholesterol display strong NIR-II fluorescence and can be capsulated with the PEGylated lipid into BP@lipid-PEG nanoparticles for NIR-II optical imaging.	[80]
BPNS@TA-Mn	PAI/MRI/PTT	HeLa tumor	It applies PAI/MRI dual-mode imaging for guided PTT.	[81]
MUCNPs@BPNS-Ce6	MRI/PAI/ultrasound/fluorescence/PTT/photodynamic (PDT)	HeLa tumor	The multi-functional layered-BP platform can simultaneously implement four imaging modalities and two treatment schemes; the agent has strong absorption of NIR light for deep tissue applications.	[82]
NB@BPs	PTT	MCF7 breast tumor	A Nile Blue (NB) diazonium tetrafluoroborate salt is covalently doped with BPs, enhancing the stability.	[83]
NIR-II-CD/BP	PTT	4T1 tumor	NIR-II-CD/BP show remarkably enhanced photothermal conversion efficacy and antitumor efficiency in NIR-II region, the most suitable optical window for clinical use.	[84]
MTP-BP-al-PEG	PTT	4T1 tumor	Targeting to higher potential membrane and mitochondria of cancer cells greatly boost the PTT efficiency.	[85]

(Continued)

material	application	disease	highlight of the research	Ref.
BPQDs/GA/PLLA-PEG-PLLA	PAI/PTT	T47D tumor	Gambogic acid inhibits heat shock protein expression conducting a better PTT effect.	[86]
PEGylated BPQDs	PDT	S180 tumor	It demonstrates the good stability, no cytotoxicity and PDT potential of BP.	[87]
Cy5-dHeme-BPNS-FA	PDT	HeLa tumors	The excessive intracellular H ₂ O ₂ were catalyzed with passivated BP-based nanoplatform to generate O ₂ that is essential for PDT, leading to significant enhancement of PDT efficacy for tumor treatment.	[88]
BP-DOX	PDT/PTT/ chemotherapy	4T1 tumor	The drug loading rate of layered-BP is increased by up to 9.5 folds.	[89]
BP@hydrogel	chemotherapy	MDA-MB-231 tumors	By loading DOX in the layered-BP modified with hydrogel, laser exposure can be regulated to release drugs to treat cancer.	[90]
BP-DOX@PDA-PEG-FA	PTT/chemotherapy	Hela tumor	BP-DOX@PDA-PEG-FA combined with laser irradiation yields dramatic synergistic antitumor effects, inducing no acute side effects.	[91]
BP-R-D@PDA-PEG-Apt	genetherapy/ chemotherapy/PTT	MCF-7 tumor	BP can be used in targeted chemo, PTT, and gene against multidrug-resistant cancer.	[92]
BSPTD	chemotherapy/ PTT/ fluorescence	4T1 tumor	It can specifically target the tumor site, and inhibit metastasis during the targeting chemo-photothermal therapy, benefiting from the secondary drug delivery facilitated by photothermal degradation.	[93]
RV/CAT-BP@MFL	fluorescence/PTT/ PDT/chemotherapy	MCF-7 tumor	It displays folate receptor-targeted delivery, tumor hypoxia relief, and synergistic suppression of tumorous cell propagation.	[94]
BPNVs-CpG	PDT/immunotherapy/ PAI	4T1-tumor	It enhances deeper tumor penetration synergized immunotherapy induced by CpG, yielding an excellent cancer therapy effect.	[95]
R-MnO ₂ -FBP	MRI/fluorescence/ PDT	HeLa tumor	It demonstrates a dual-mode of fluorescence imaging and MR imaging for guided PDT.	[96]
NE hydrogel	osteanagenesis	calvarial defect	It demonstrates BP nanosheets-based nanoengineered hydrogels can increase biological mineralization and promote bone osteogenic cell differentiation and bone regeneration.	[97]
BPNs/chitosan/PRP	osteanagenesis/ PTT/PDT	rheumatoid arthritis	Platelet-rich plasma-chitosan was combined with BP which induced calcium-extracted biomineralization and phototherapy, getting a better curative effect of rheumatoid arthritis.	[98]
BP@PDA-incorporated GelMA scaffold	MSC differentiation		It can significantly promote the differentiation of mesenchymal stem cells (MSC) into neural-like cells under the synergistic electrical stimulation.	[99]
BP nanosheets	Cu ²⁺ regulation	neurodegenerative disorder	BP nanosheets are promising neuroprotective nanodrug for NDs because they process preminent photothermal effect, increasing its blood-brain barrier permeability and subsequently act as a chelator to regulate Cu ²⁺ concentration.	[100]
PEG-LK7@BP	Cu ²⁺ regulation /chemotherapy	Alzheimer's disease	BP can efficiently bind with the peptide inhibitor LK7 to inhibit amyloid formation.	[101]
BP nanosheets	antioxidative therapy	acute kidney injury	BP nanosheets are easily to be oxidized into phosphorus oxides which can act as promising antioxidative agents for consuming excess cytotoxic reactive oxygen species.	[102]

3 Functionalized layered-BP nanoparticles and their applications

Phosphonate and phosphate, both being nontoxic, are the final products of BP degradation. BP nanoparticles have admirable biocompatibility and distinguished photothermal performance; hence, they are promising for biomedical applications. A wide variety of nanomaterials based on the layered-BP platform have been developed for the diagnosis and treatment of various diseases (summarized in Table 2).

Notably, BPNs are good absorbents for PA imaging (PAI) and PTT because they can convert light into heat effectively. BP can also effectively produce reactive oxygen species (ROS) after absorbing light, making it a good candidate agent for PDT. In addition, BPNs has the potential for drug-loading applications due to its comparatively large surface area. It is also used to load therapeutic agents in chemotherapy and combinations of different treatments, such as chemotherapy, PTT, and gene PDT. Such combined therapies exhibit advantages of relatively

few side effects and high therapeutic efficacy. Although immense progress has been made, a major obstacle to the application of layered BP is the material degradation under long-time exposure in the natural environment. The main reason for the degradation is the PO_x produced by oxygen reaction with the lone pair electrons perpendicular to the BP surface. To overcome this obstacle and improve the performance of layered BP, various strategies have been designed, such as vdW, covalency, and electrostatic functionalization. Ideal functionalization can strengthen the stability of layered BP and maintain or enhance its particularity for long-term use [18]. In 2017, Tao et al. designed a layered-BP-based theranostic delivery platform (Fig. 2(a)) and investigated its biological activities by tracing the endocytosis pathways in tumor cells for the first time; their study demonstrated the potentials of BP-based delivery platforms in cancer diagnosis and therapy [32]. Further, the layered BP was synthesized by mechanical cleavage, followed by functionalization with positively charged polyethylene glycol-amine (PEG-NH₂) by electrostatic adsorption to enhance the physiologic stability and biocompatibility. The team revealed that the PEGylated layered BP was taken up by cells via caveolae-dependent endocytosis, particularly the macropinocytosis pathway (Fig. 2(b)). Finally, they were degraded in lysosomes by classic endocytosis pathways or autophagy. This PEGylated layered BP can be used to efficiently load heat-soluble drugs, such as doxorubicin (DOX) for chemotherapy and cyanide (Cy7) for *in vivo* NIR imaging.

3.1 Multifunctional layered-BP nanoparticles for diagnostic imaging

Achieving precise diagnosis and effective treatment of tumors is a key and urgent problem in biomedicine [103]. After the combination with metallic elements, metal phosphates/phosphate nanomaterials are particularly suitable for tumor imaging based on modalities (e.g., magnetic resonance imaging (MRI), fluorescence imaging (FI), and PAI). Among them, PAI has many proven advantages over traditional optical imaging modalities, e.g., depth-resolved 3D imaging, higher sensitivity and image contrast, and higher spatial resolution with depths of up to a few centimeters [104,105]. BP is inherently promising for boosting PAI-based diagnosis, due to its innate strong and wide absorption property [106]. Moreover, surface modifications, e.g., with titanium ligand or PEG, can stabilize BP in aqueous dispersions. It has been reported that PA signals of $\text{TiL}_4\text{@BPQDs}$ at a concentration of as low as 22.0×10^{-6} are nearly 7.29 times higher than those of Au nanoparticles at a concentration of 79.8×10^{-6} , adequately demonstrating the excellent performance of $\text{TiL}_4\text{@BPQDs}$ [30]. In another work, BP was modified with branched poly(ethyleneimine) (PEI) and dextran (DEX) to achieve biocompatibility, as well as with folic acid (FA) for tumor targeting [79]. These biocompa-

tible and water-soluble BPNPs (BP-DEX/PEI-FA) can improve the *in vivo* PA signals of tumor imaging to 3.1 times higher than those of pre-contrast images (Figs. 3(a) and 3(b)). BP also exhibits potentials in the second NIR (NIR-II) FI that yields lower autofluorescence and deeper penetration (due to the lower optical scattering and absorption in biological tissues) than NIR-I FI [107,108]. In 2019, Xu et al. first demonstrated that layered BP modified with cholesterol and encapsulated with PEGylated lipid into nanospheres (BP@lipid-PEG) shows strong fluorescence for NIR-II imaging [80]. After the injection of BP@lipid-PEG nanospheres, the surficial blood vessels and liver could be readily observed (Fig. 3(c)), and even tiny branched vessels marked with the yellow dotted lines could be observed under the images at 30 s post-injection with 1250 and 1400 nm optical filters (Fig. 3(d)).

Note that the single-mode imaging method is often inadequate and does not meet the requirements of specificity and targeting. Thus, molecular probes are required for multimode molecular imaging, which can overcome the limitation of single-mode imaging, achieve complementary functions, and broaden the applications. The multimode imaging probes can be developed via various methods. For example, using facile tannic acid as the chelating agent, paramagnetic Mn^{2+} can be added to the layered BP to achieve high-resolution PAI/MRI dual-mode imaging that enables deep-tissue penetration for tumor detection [81]. In 2019, a multimodal imaging agent suitable for MRI, PAI, fluorescence, and ultrasonic imaging was fabricated by modifying layered BP with chlorin e6 (Ce6) and $\text{Fe}_3\text{O}_4\text{@MnO}_2\text{-doped NaYF}_4\text{:Yb/Er/Nd}$ upconversion nanoparticles (UCNPs) [82]. By absorbing long-wavelength photons (considerably deep-tissue penetration), the UCNPs can emit high-energy short-wavelength light for photosensitizer activation, thereby promoting the success rate of the therapy [109]. The preparation of such BP-based nanopatforms is illustrated in Fig. 4. As shown, layered BP is first obtained by liquid exfoliation. To obtain hydrophilic magnetic UCNPs (MUCNPs), layered BP is modified with strong coordinated poly(acrylic acid). Thereafter, it is coated with polylysine by electrostatic interaction for enhanced stability and combined with MUCNPs via chemical-bond cross-linking. Last, Ce6 is loaded on the nanopatform to improve the sensitizing efficacy. The obtained MUCNPs@BPNs-Ce6 demonstrates remarkable light-conversion efficiency, imaging properties, and biocompatibility. Moreover, the layered-BP-based nanoparticles can be used not only for diagnosis before treatment but also for monitoring during treatment and evaluation after treatment.

3.2 Multifunctional layered-BP nanoparticles for PTT

With varying layer-dependent bandgap, layered BP exhibits broadband absorption even in infrared regions,

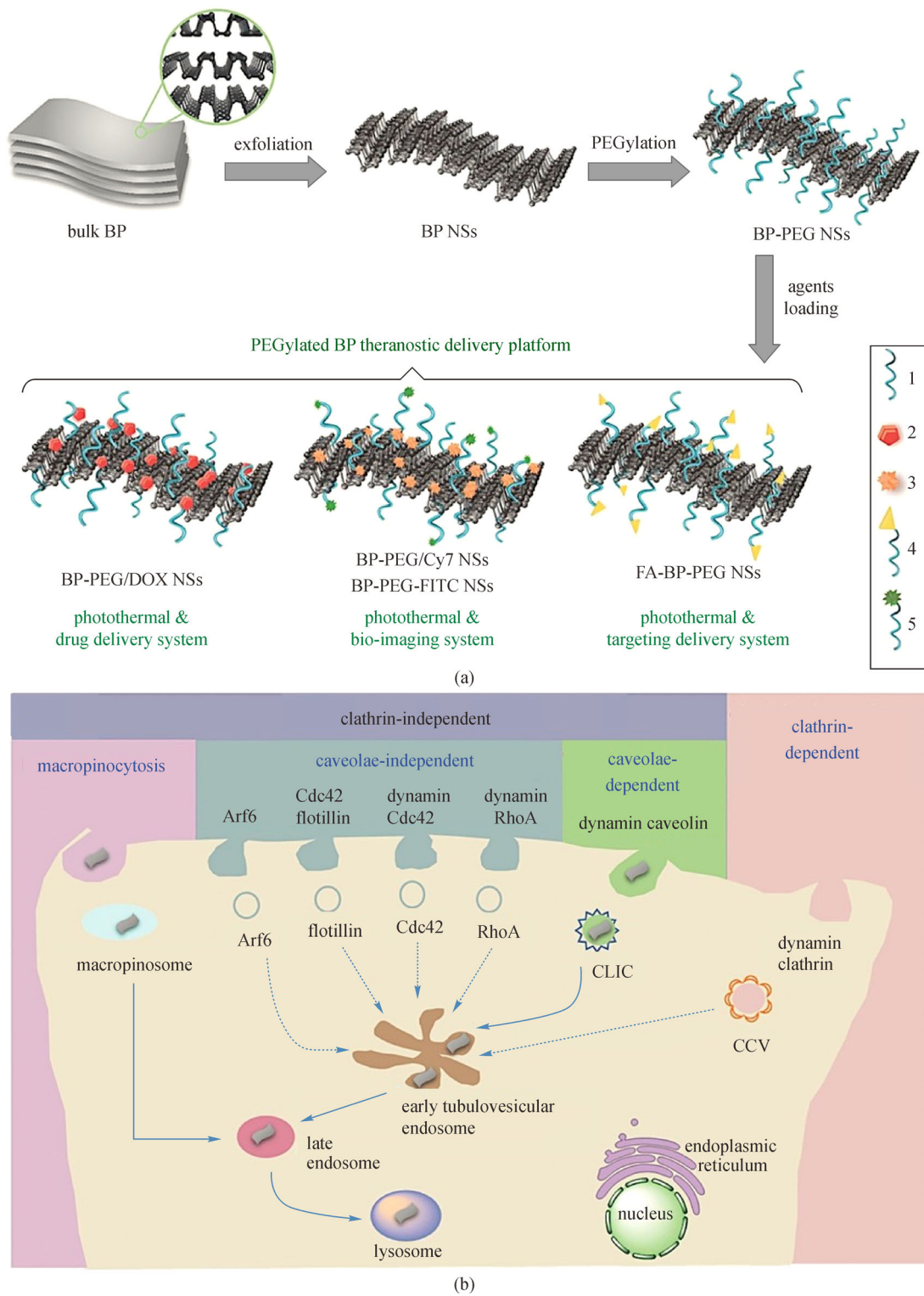


Fig. 2 (a) Preparation of the PEGylated BP theranostic delivery platform. 1: PEG-NH₂ (surface modification), 2: DOX (therapeutic agents), 3: Cy7-NH₂ (NIR imaging agents), 4: FA-PEG-NH₂ (targeting agents), 5: FITC-PEG-NH₂ (fluorescent imaging agents). (b) Screening and summary of the endocytosis pathways and the biological activities of PEGylated BPNSs in cancer cells. Reproduced from Ref. [32]

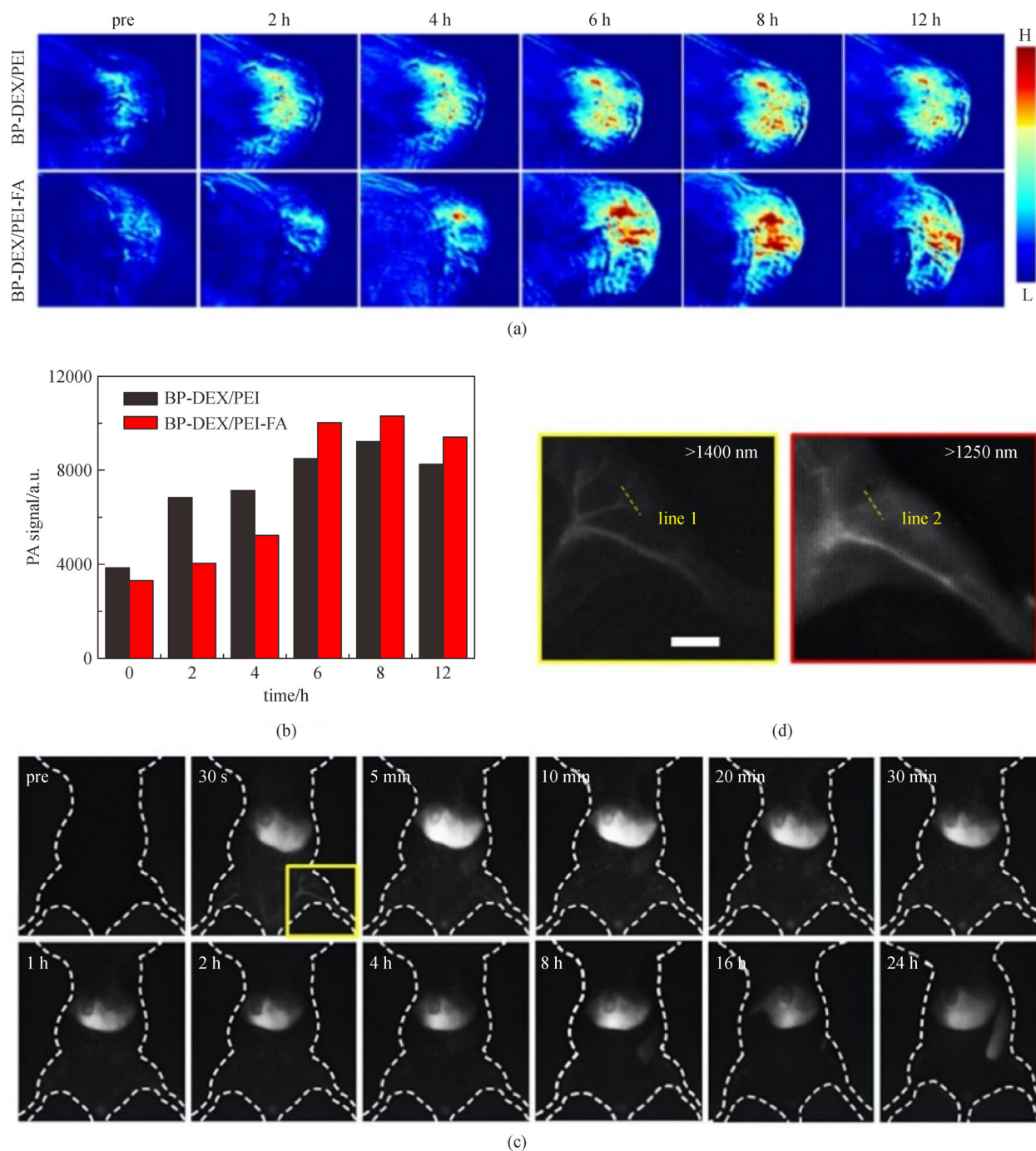


Fig. 3 (a) and (b) Targeted imaging of tumors with BP-DEX/PEI-FA nanoparticles. (a) *In vivo* PA images of the 4T1 tumor-bearing mice before and after tail vein injection of BP-DEX/PEI and BP-DEX/PEI-FA nanoparticles (2 mg/mL) at different time points. (b) PA signal intensities of the tumors from the 4T1 tumor-bearing mice collected at different time points after tail vein injection of BP-DEX/PEI and BP-DEX/PEI-FA nanoparticles. (c) *In vivo* NIR-II fluorescence images of a mouse collected at different time intervals using a 1400-nm optical filter after intravenous injection of BP@lipid-PEG nanosphere aqueous solutions. (d) Enlargement of the image acquired at 30 s post-injection with different optical filters (1400 and 1250 nm, respectively). Scale bar = 5 mm. Reproduced from Refs. [80,107]

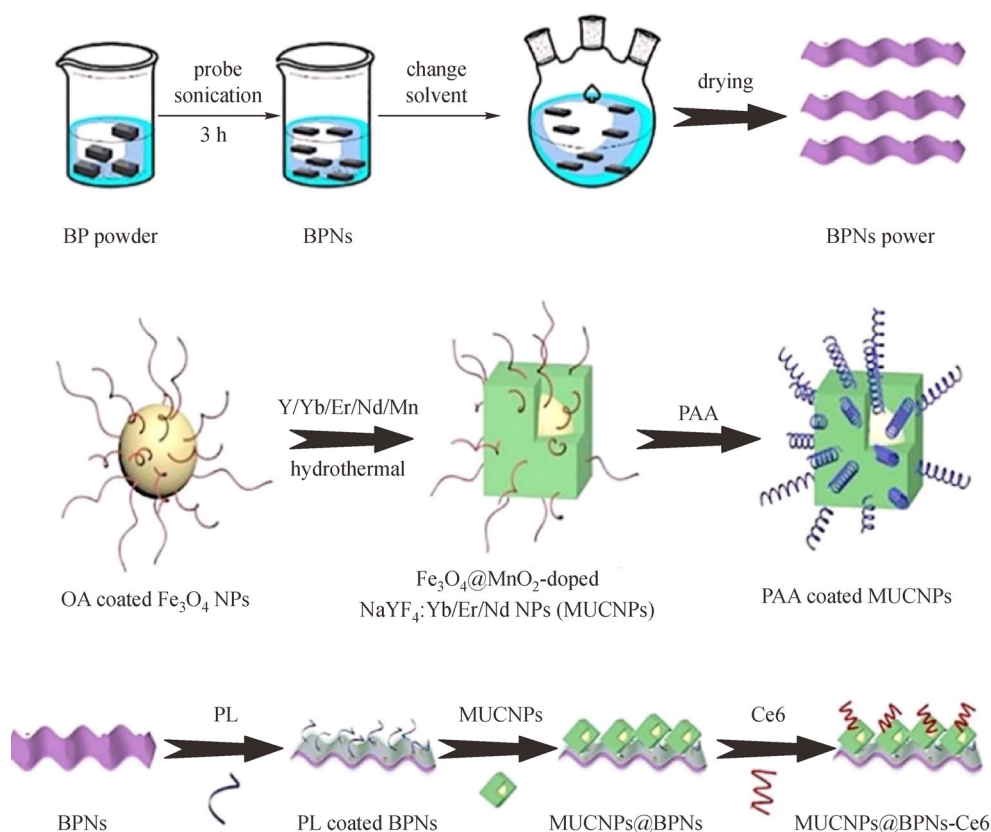


Fig. 4 Schematic illustration of the fabrication of BP-based nanoplatforms (MUCNPs@BPNs-Ce6). Reproduced from Ref. [109]

making it a promising platform for PTT. For example, in 2017, Zhao et al. covalently modified layered BP with an NB diazonium tetrafluoroborate salt (NB-D) to prevent rapid degradation (Fig. 5(a)) [83]. The stability of NB-D covered layered BP (NB@BP) was obviously higher than that of bare layered BP, regardless of the morphological changes, absorbance intensity, temperature rise, or emission intensity ratio (Figs. 5(b) and 5(c)). The peak-absorbance intensity of NB@BP decreased by only 3% after 3 days of dispersion in water and exposure to air (Fig. 5(d)). Under the premise of maintaining stability, the effect of PTT *in vivo* is satisfactory as expected; the tumors shrink gradually, and complete recovery is achieved within 16 days of treatment (Fig. 5(e)).

In 2019, Geng et al. designed a hybrid photothermal agent by loading a carbon dot, which is responsive to NIR-II light (NIR-II-CD), on the surface of layered BP, thereby achieving eminent photothermal conversion efficiencies of 77.3% and 61.4% in the NIR-I and NIR-II windows, respectively [84]. This is important for clinical applications because the NIR-I region (700–1000 nm) and NIR-II region (1000–1350 nm) can be used to selectively destruct deep tumors without damaging neighboring normal tissues

[110,111]. By covering the NIR-II-CD/BP nanoparticle with a piece of chicken breast tissue of varying thicknesses (2–10 mm), its PTT effectiveness in deep tissue was evaluated using an 808- or 1064-nm laser (Fig. 6(a)). Under the 1064-nm laser irradiation, reduced attenuation of temperature and increased T_{\max} of the NIR-II-CD/BP nanoparticles were achieved (Figs. 6(b) and 6(c)). Notably, the temperature of the NIR-II-CDs/BP nanoparticle increased by 22.0°C under the 1064-nm laser irradiation when the tissue depth was 10 mm, whereas it only increased by 12.5°C under the 808-nm laser irradiation (Fig. 6(d)). The *in vivo* experiments verified that the 4T1 tumor-bearing mice can be cured after 18 days of PTT under 1064 nm laser irradiation, even though chicken breast tissue was covering the tumor sites.

Recently, a strategy for the specific identification of cancer cells to improve PTT efficiency was developed. Layered BP was functionalized with a mitochondria-targeting peptide because mitochondria are more abundant in cancer cells than in normal cells [85]. Mitochondria injuring could induce multiple regulatory processes including cell death would be triggered by caspase-3 proteins and cytochrome when they are released into the

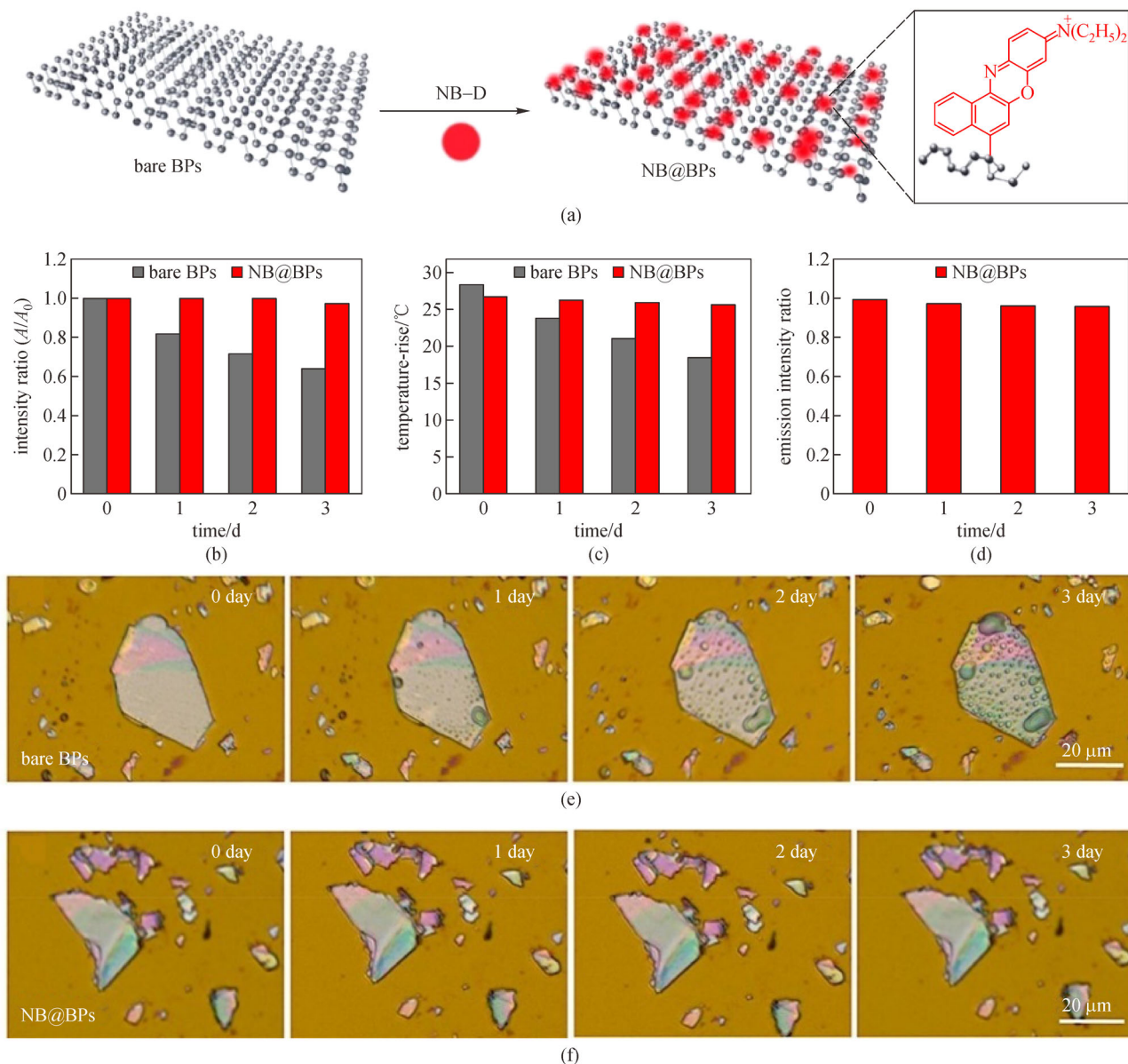


Fig. 5 (a) Schematic illustration of the fabrication of NB@BPs. (b)–(f) Material stability examinations. Time-dependent variations in the (b) absorption ratios at the respective peak wavelength (A/A_0) and (c) increase in the temperature of the bare BPs and NB@BPs in water under 808 nm and 1.0 W/cm^2 laser irradiations for 10 min. (d) Time-dependent variations of the fluorescence intensity of NB@BPs in water. Optical images of micro-sized (e) bare BPs and (f) NB@BPs exposed under ambient conditions for different dispersion time lengths. Reproduced from Ref. [83]

cytoplasm. Furthermore, modification with acid-labile PEG for stability can boost the accumulation of BP in the tumor tissue due to the slightly acidic environment of tumor tissue, thereby increasing the efficiency of cancer therapy.

Although cells can die from overheating, they have inherent regulatory mechanisms for coping with overheating. Up-regulating the heat shock protein (HSP) expression can improve the efficiency of PDT by elevating the heat stress tolerability. Chen et al. found that extracted gambogic acid (GA), an HSP inhibitor, can enhance the

tumor ablation effect induced by BP [86]. *In vivo* experiments showed that under irradiation, the HSP expression in the tumor cells of mice with GA-modified BP decreased by more than half compared with that of mice without GA-modified BP, resulting in enhanced therapeutic efficiency (Fig. 7).

3.3 Multifunctional layered-BP nanoparticles for PDT

PDT combines light and a photosensitive agent to selectively damage the target tissue [112]. The ROS

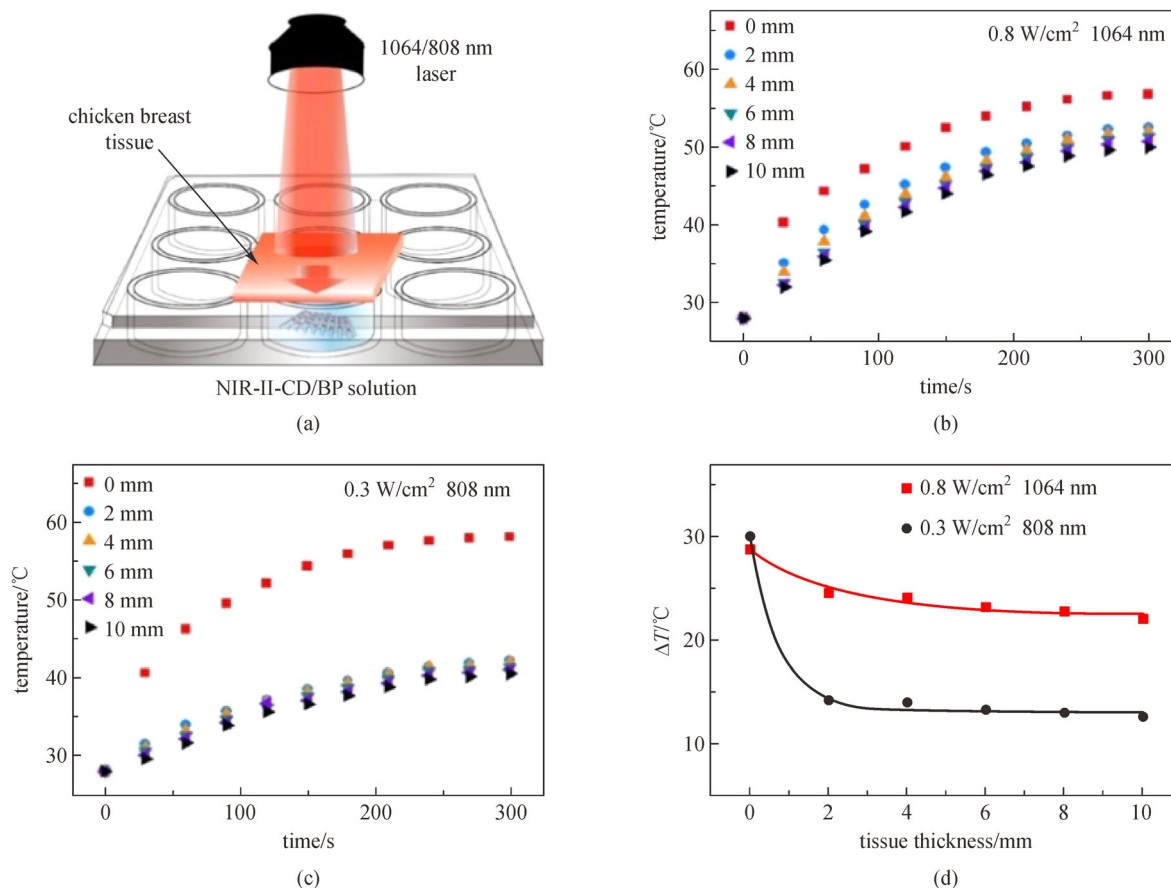


Fig. 6 (a) Schematic illustration of *in vitro* deep-tissue PTT. (b) and (c) Temperature change of the NIR-II-CD/BP solution irradiated by an 808- or 1064-nm laser in the presence of varied thicknesses of additional tissue. (d) Fitted temperature change exponential decay of NIR-II-CD/BP hybrids upon 808- and 1064-nm laser irradiations. Reproduced from Ref. [84]

produced in the PDT process, including highly reactive ions and free radicals, have been shown to destroy tumors effectively. PDT has a direct effect on cancer cells, leading to cell death through necrosis and/or apoptosis. PDT also influences the tumor vascular system with light and ROS production; this leads to vessel closure, thereby depriving the tumor of oxygen and nutrients [113]. Because of its unique electronic structure, BP can be used as an effective photosensitive agent to generate ROS under light irradiation for the PDT of tumors (Fig. 8(a)). In 2015, Wang et al. first demonstrated that BPNSs were outstanding photosensitizers with a high quantum yield of ~ 0.91 , which is higher than those of most PDT agents reported earlier [33]. Later, to enhance the stability in various media, Guo et al. modified the layered BP with PEG through electrostatic adsorption [87]. PEG-modified BP can remain stable in water, phosphate-buffered saline (PBS, pH 7.4), cell culture media, and fetal bovine serum for over at least 30 days (Fig. 8(b)). After being incubated with L02 or HeLa cells for 24 h, both naked layered BP and PEG-lized layered BP showed no appreciable cytotoxicity even at the highest concentra-

tion ($40.5 \mu\text{g/mL}$), demonstrating the favorable biocompatibility of BP (Fig. 8(c)). In addition to photosensitization and irradiation, oxygen is also essential for PDT. Most PDT applications rely on *in situ* oxygen to complete the treatment process; however, oxygen is very limited. In this case, Liu et al. designed a layered-BP-based oxygen self-supply photosensitizer (Cy5-dHeme-BPNS-FA) with the functionalization of DNA duplex and FA [88]. Integrating Fe-protoporphyrin IX (Heme) as the catalyst with BPNSs can help locally or site-specifically convert hydrogen peroxide (H_2O_2), which is excessive in cancer cells, to singlet oxygen to enhance PDT. In *in vitro* oxygen self-supply effect evaluation, the cell apoptosis proportion of Cy5-dHeme-BPNS-FA cultured cancerous cells is 8.7-fold higher than that of the control group without Heme under hypoxia condition. For the *in vivo* experiment, the tumor volume of animals treated with Cy5-dHeme-BPNS-FA and PDT drastically declined to 6% of the tumor volume before treatment (Figs. 8(d) and 8(e)). Both *in vitro* and *in vivo* experiments demonstrate that this layered-BP-based photosensitizer significantly boosts the treatment effect of hypoxic tumors.

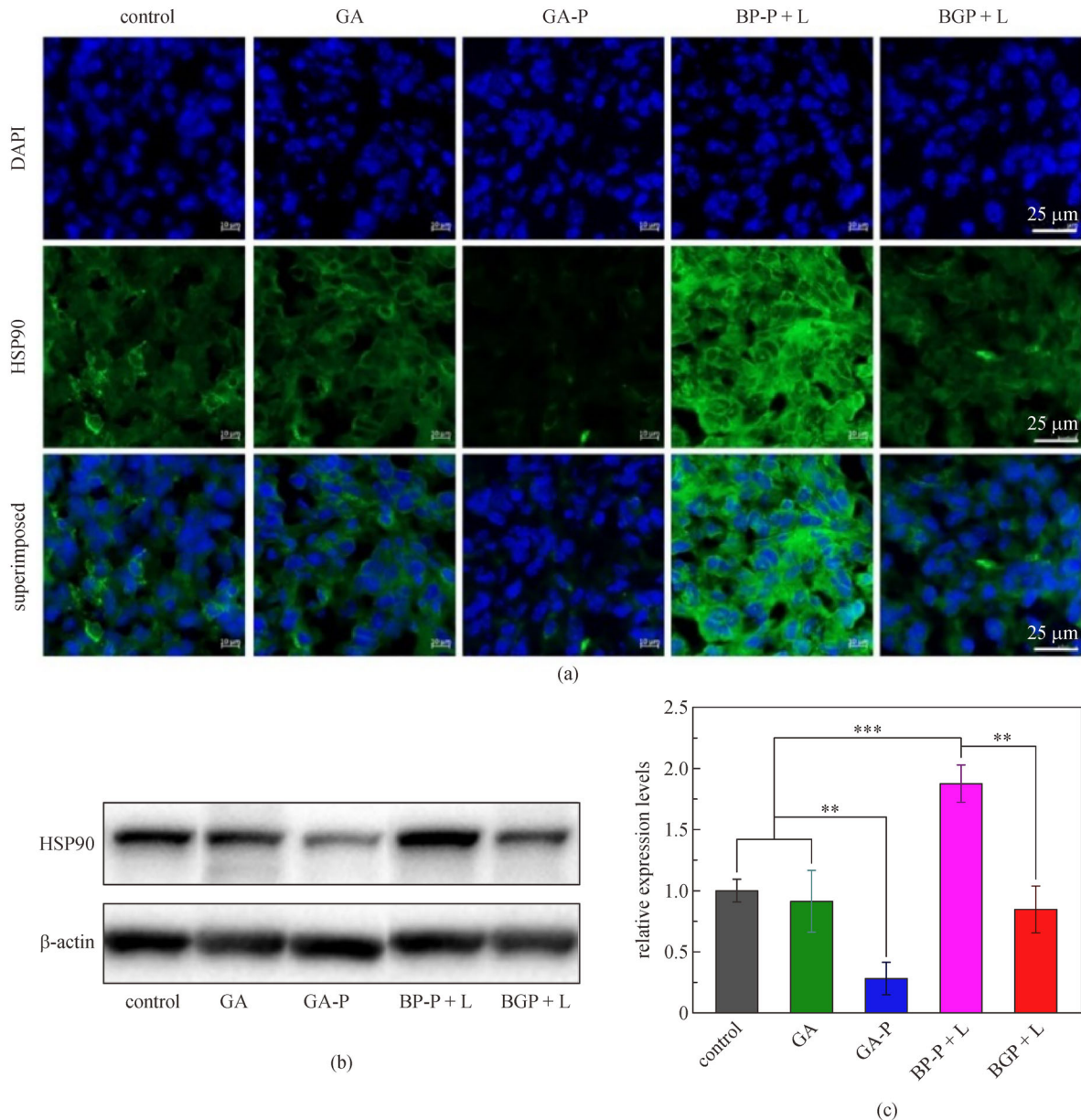


Fig. 7 (a) HSP90 expressions in tumors collected from mice 2 days after applying various treatments, as determined by immunofluorescence staining. (b) Western blot data of T47D tumor lysates collected from mice 2 days after applying various treatments. (c) Relative expression of HSP90 normalized against β-actin (control). ** $P < 0.01$, *** $P < 0.001$. Reproduced from Ref. [86]

3.4 Multifunctional layered-BP nanoparticles for drug delivery

With the increase in the understanding of cancer development, a variety of chemotherapy drugs have been developed to treat different types of cancer. Though chemotherapy plays an important role in clinical practice, the side effects of chemotherapeutic drugs are ineluctable. The application of the delivery nanoplatform to control the release of chemotherapeutic drugs and reduce their potential toxicity has been studied for decades [114].

Compared with traditional chemotherapeutic drugs, the layered-BP-based delivery nanoplatforms have the advantages of higher load efficiency, longer cycle time, stronger tumor-targeting ability, and fewer side effects. For example, in 2017, Chen et al. combined a positive anticancer drug, DOX, and negative BP by electrostatic interaction to make a layered-BP-based drug delivery nanoplatform for cancer treatment [89]. Because of the large surface area of layered BP, it could hold larger amounts of DOX on the sheet surface (950% in weight) than other reported 2D material systems. Although this

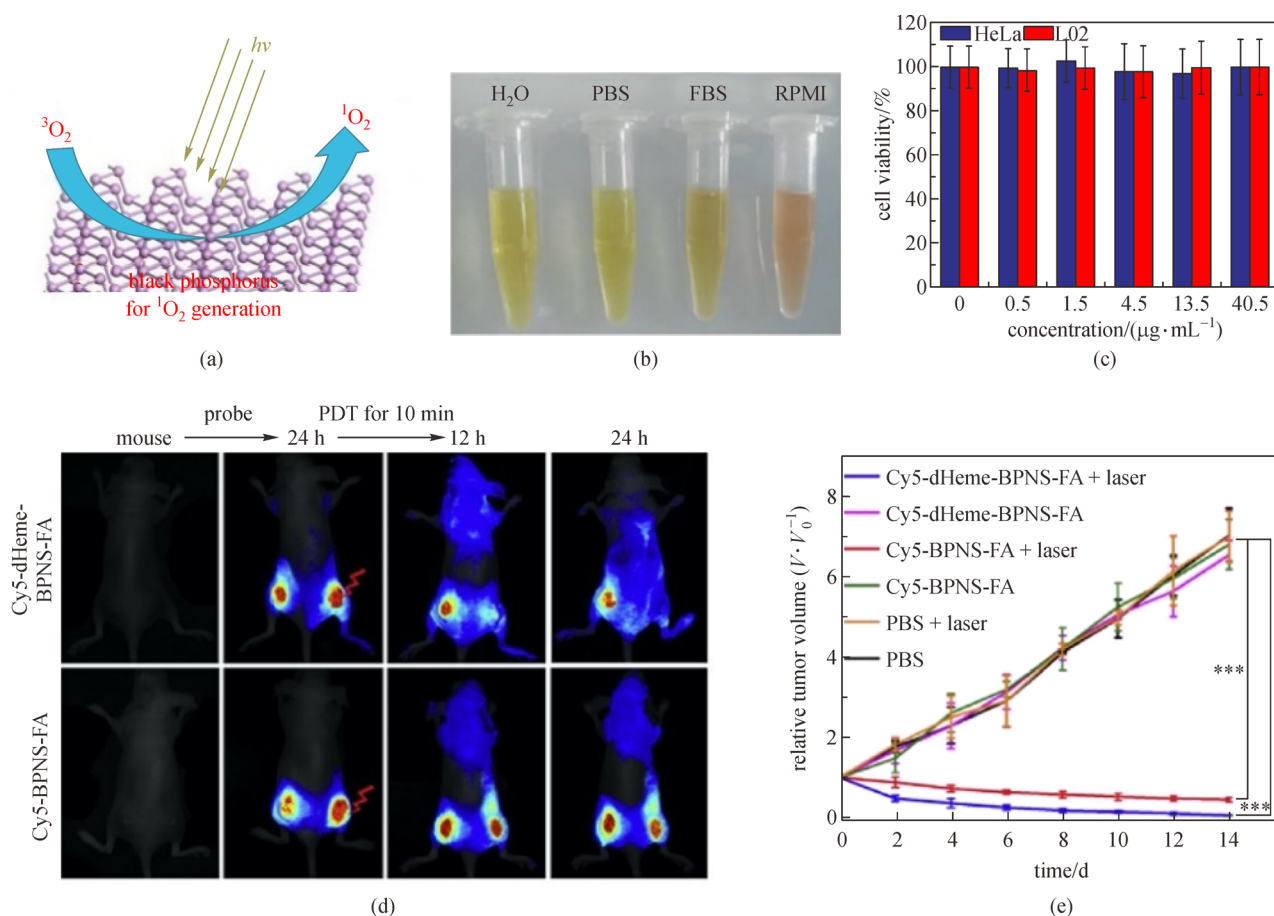


Fig. 8 (a) Schematic illustration of singlet-oxygen production by BPNSs under laser irradiation. (b) Photographs of PEGylated BPQDs dispersed in various media. (RPMI refers to RPMI 1640 media) (c) Cell viability of HeLa and L02 cells after incubation with BPQDs at different concentrations at 37°C for 24 h. (d) *In vivo* imaging monitoring of the PDT effect on tumor-bearing mice in both the left and right flanks after the injection of Cy5-dHeme-BPNS-FA or Cy5-BPNS-FA. After 24 h post-injection, the tumor in the right flank was irradiated with laser, whereas the tumor in the left was kept away from light as the control. (e) Relative change of the averaged tumor volume after treatment with PBS, Cy5-dHeme-BPNS-FA, and Cy5-BPNS-FA with and without laser irradiation. Statistical analysis was performed using Student's *t*-test (** $P < 0.01$ and *** $P < 0.001$). Reproduced from Refs. [87,88,113]

method greatly improved the treatment efficiency of anticancer drugs, it was difficult to control the rate of drug release and predict the dosage and treatment effect. In 2018, Qiu et al. developed a BP-containing hydrogel platform (BP@hydrogel) with BP embedded in low-melting agarose [90]. After loading DOX in the BP@hydrogel, it could be regulated by laser exposure to release drugs to treat cancer. When BP absorbs light and converts it to thermal energy, the agarose hydrogel undergoes reversible hydrolysis and softening, resulting in accelerated drug diffusion from the platform to the surrounding environment (Fig. 9(a)). The results were verified in mouse subcutaneous breast and melanoma models. In addition, Gao et al. designed BP-DOX@PDA-PEG-FA, where the BPNS surface was modified with polydopamine (PDA) for stabilization and with FA for tumor targeting [91]. The cell viability was assessed on HeLa cells incubated with

BP-DOX@PDA-PEG-FA, and it decreased with the increase in the concentration of DOX. DOX showed higher cytotoxicity than the DOX-loaded BP-based nanoparticles, because it directly entered the nucleus, whereas the BP-based nanoparticles required some time for the release of the loaded DOX. The BP-DOX@PDA-PEG-FA with profound tumor-targeting and photothermal effects had a more significant ablation effect than other forms of the BP-based nanoparticle (Fig. 9(b)). The *in vivo* therapeutic effect was also tested on mice xenograft tumor models. BP-DOX@PDA-PEG-FA combined with laser irradiation displayed dramatic synergistic anti-tumor effects without inducing any acute side effects. Both the groups of DOX and BP-DOX@PDA-PEG-FA displayed significant tumor growth suppression. Among all the groups, the BP-DOX@PDA-PEG-FA with NIR laser-exposure group exhibited the lowest tumor growth rate and

best anti-tumor effect, which can be attributed to the synergistic effect of chemotherapy and PTT and the tumor-targeting effect (Fig. 9(c)).

3.5 Functional layered-BP nanoparticles for multifunctional co-delivery

A single treatment approach may not effectively control tumor progression considering the high malignancy probability. Generally, chemotherapy is associated with toxicities, side effects, and drug resistance, which would significantly reduce therapeutic effectiveness [115,116]. Moreover, the low targeting effect of PTT also reduces the treatment efficiency [117]. As discussed earlier, imaging probes and therapeutic agents can be integrated to exploit the diagnostic and therapeutic functions simultaneously. Further, the application of multifunctional molecules in

tumor therapy can enhance the tumor-targeted transmission of drugs. In addition, real-time observation of the distribution and metabolism of drugs in the body can be realized. Personalized treatment can be adjusted timely according to the real-time monitoring of the treatment progress and evaluation of the drug efficacy. This strategy can improve the safety and efficiency of tumor treatment. Therefore, in recent years, multidisciplinary combination therapy has become a trend in tumor therapy. Several representative examples are discussed as follows.

In 2018, Zeng et al. designed multifunctional layered-BP-based nanoparticles for targeted chemo/PTT/gene against multidrug-resistant cancer [92]. The anticancer drug, DOX, was loaded after permeability glycoprotein (P-gp) siRNA adsorption onto the BP surface. PDA was modified to enhance the ambient stability. P-gp siRNA can down-regulate the expression of P-gp on the cancerous cell

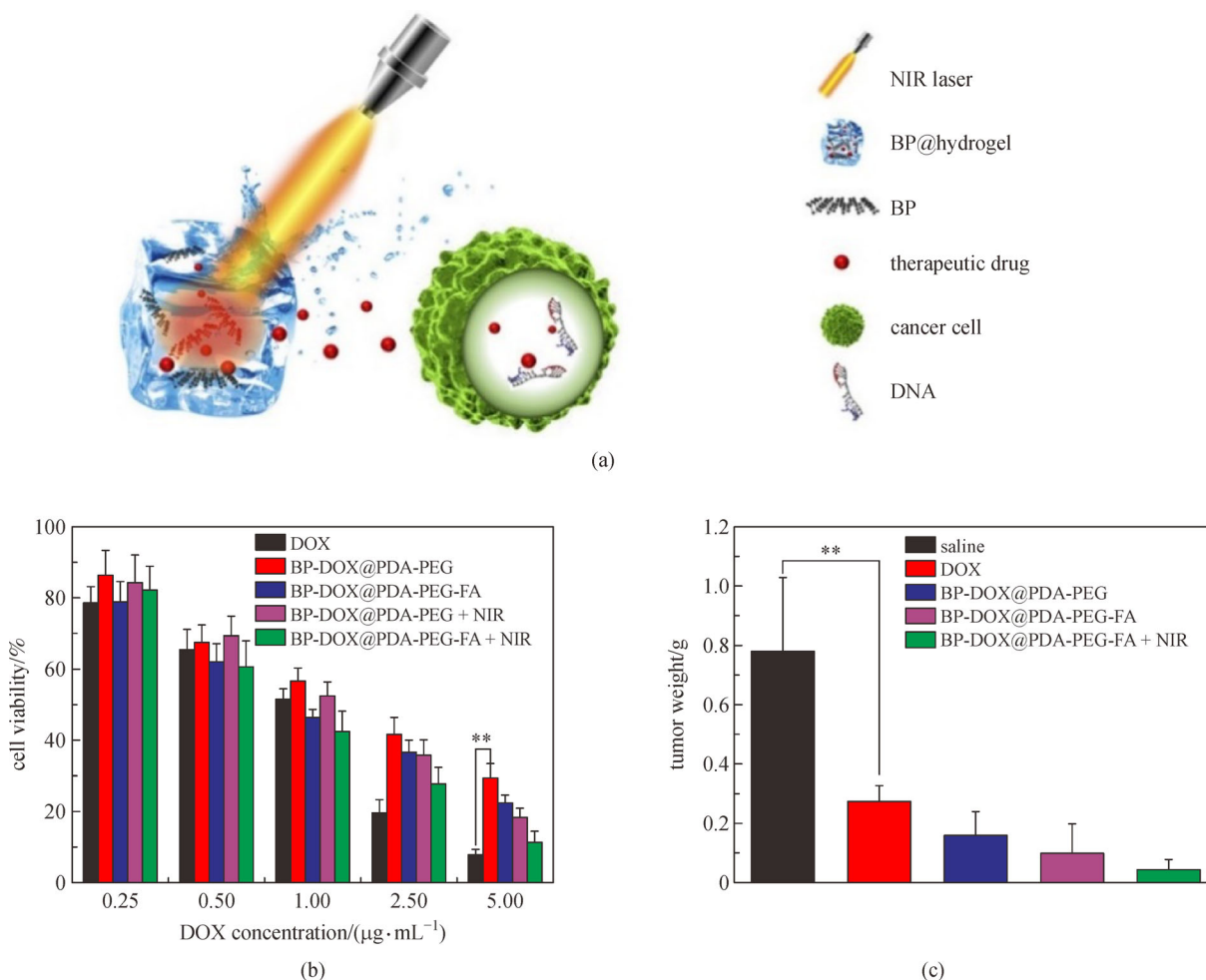
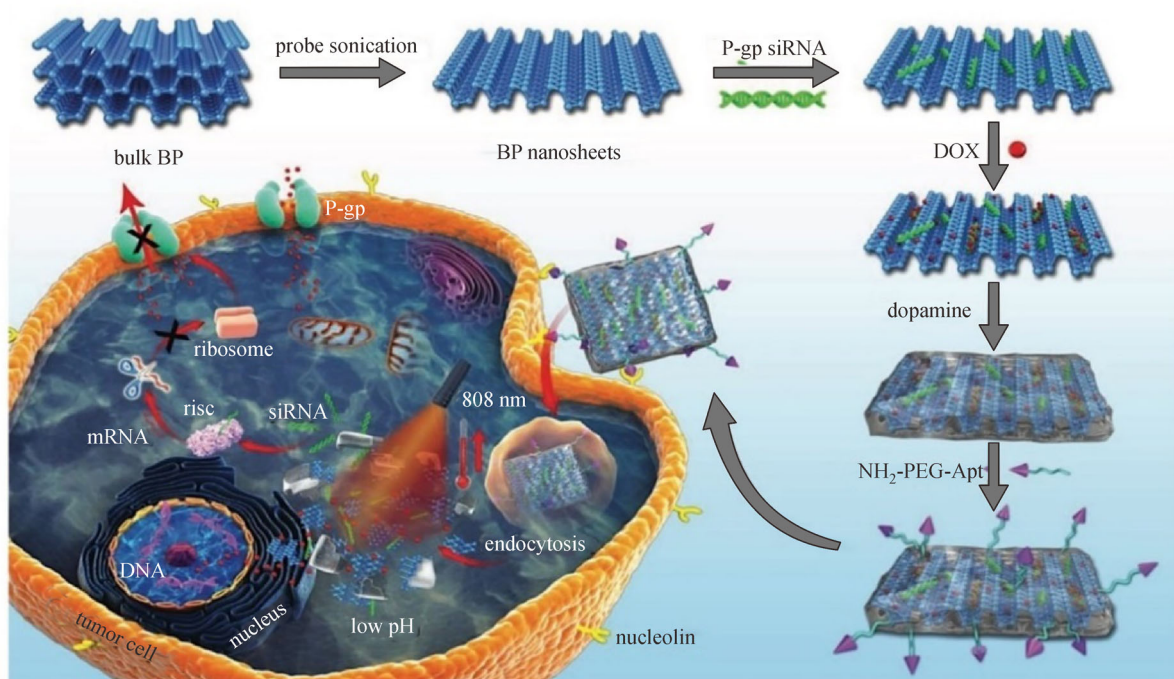


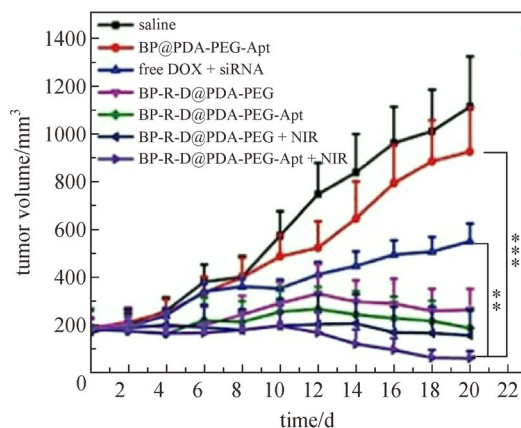
Fig. 9 (a) Schematic illustration of the working principle of BP@hydrogel. BP@hydrogel releases the encapsulated chemotherapeutics under NIR-light irradiation to break the DNA chains, thereby inducing apoptosis. (b) Viability of HeLa cells cultured with DOX-loaded nanoformulations in comparison with that of free DOX at the same DOX dose after 24 h (** $P < 0.01$). (c) Anti-tumor efficacy of saline, DOX, BP-DOX@PDA-PEG, BP-DOX@PDA-PEG-FA, and BP-DOX@PDA-PEG-FA + NIR on the nude mice bearing HeLa cell xenografts. Tumor weight of each group was obtained from the sacrificed mice at the end of the study (** $P < 0.01$). Reproduced from Refs. [90,91]

membranes, inducing P-gp-mediated multidrug resistance. Finally, BP-R-D@PDA-PEG-Apt nanoparticles were synthesized after introducing NH₂-PEG-Apt, resulting in high tumor-targeting ability, biocompatibility, and physiologic stability (Fig. 10(a)). From the results of the *in vitro* tests, the DOX release rate was as high as 46.9% under the condition of pH 5.0 after four cycles of irradiation. BP-R-D@PDA-PEG-Apt reduced the P-gp expression by 68% and showed a significant temperature increase, indicating that the multifunctional platform can perform well. The *in vivo* test on mice showed that multimodal therapy can destruct the tumor with better performance than single-mode therapy in inhibiting the tumor cell proliferation

(Figs. 10(b) and 10(c)). Quite recently, a synergistic therapeutic agent, DOX-loaded BSPT-based system (BSPTD), based on layered-BP was synthesized to specifically target tumor tissue after modification with TKD peptide (targeting ligand that binds to the memHsp70 receptor, which is overexpressed in malignant tumors) [93]. However, instead of using layered BP directly as a carrier of DOX here, mesoporous silica acted as the medium for the more stable BP-based drug delivery platform, and it promoted a covalent connection with PEG and TKD. Correspondingly, BSPTD achieved effective synergistic tumor-targeted treatment of lung metastasis, combining chemotherapy and PTT. They conducted an



(a)



(b)

saline
 BP@PDA-PEG-Apt
 DOX + siRNA
 BP-R-D@PDA-PEG
 BP-R-D@PDA-PEG-Apt
 BP-R-D@PDA-PEG + NIR
 BP-R-D@PDA-PEG-Apt + NIR



(c)

Fig. 10 (a) Schematic illustration of the procedure used to fabricate nanostructures and the combined chemo/gene/photothermal targeted therapy of tumor cells. (b) Inhibition of tumor growth after different treatments. (c) Morphology of tumors removed from the sacrificed mice in all groups at the end of the study (** $P < 0.01$, *** $P < 0.001$). Reproduced from Ref. [92]

interesting experiment: they compared the treatment of BSPTD with non-biodegradable graphene@mesoporous silica nanosheet-based system (GSPTD) in their work. The results showed that lung metastasis reappeared on the 21st day after treatments with GSPTD, whereas metastasis was notably suppressed after BSPTD-based therapy. They suspected that the remarkable biodegradability of BP allowed fragments containing DOX to be re-delivered to the tumor site *in vivo* via the enhanced permeability and retention effect. Their work demonstrated that BSPTD remarkably inhibited lung metastasis, attributed to a secondary drug delivery process facilitated by the photo-thermal degradation during the targeted photothermal-chemo synergistic therapy.

In 2020, Hai et al. designed multifunctional layered-BP-based nanoparticles (RV/CAT-BP@MFL) to achieve PTT, PDT, chemotherapy, and FI simultaneously [94]. After the layered BP was prepared, resveratrol (RV), serving as an anticancer drug, and catalase (CAT), used as an O₂-evolving agent, were doped on the platform by physical adsorption to accomplish chemotherapy and reformative PDT. Conversely, liposome was functionalized with a fluorescent dye (atto647) and broad-spectrum targeted ligand (folate) to form the multifunctional liposome (MFL), which can successfully encapsulate the prepared

functional layered BP (Fig. 11). As a result, a single agent embodies the functions of folate receptor-targeted delivery, tumor hypoxia relief, and synergistic inhibition of tumor cell growth. Tumor growth can be efficiently suppressed with only one dose of such an all-in-one agent administered intravenously. Modifying BP with CpG oligodeoxynucleotides opens an immunotherapy application potential. A potent photodynamic immunotherapeutic BP-based nanoparticle not only inhibits the proliferation of tumor cells, but also blocks the distant tumor growth and metastasis [95].

In 2019, Liu et al. reported that Rhodamine B (RhB)-encapsulated manganese dioxide (R-MnO₂) was designed as an oxygen supplier and an indicator of BPNSs labeled with fluorescein isothiocyanate [96]. The discharged dyes, RhB and Mn²⁺, provided fluorescence recovery and T1-weighted MR contrast for fluorescence/MR dual-mode imaging for the oxygen supply procedure. Such a nanoparticle (R-MnO₂-FBP) can not only supply oxygen for cancer PDT but also monitor the oxygen production in real-time for the irradiation treatment. As shown in Figs. 12(a) and 12(b), according to the biodistribution of R-MnO₂-FBP in the HeLa-tumor-bearing mouse from FI and MRI, the optimal duration of irradiation treatment for the subsequent efficient therapy is 28 h. To demonstrate the

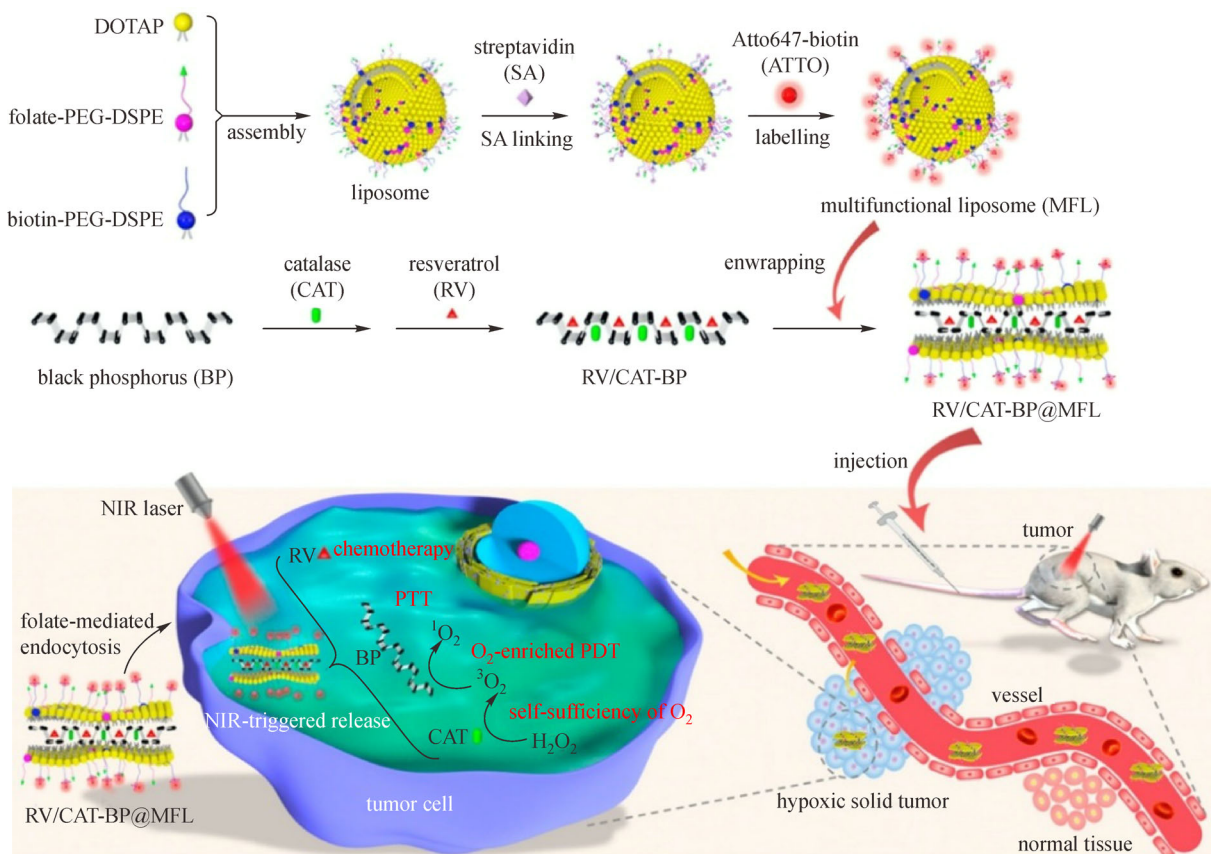


Fig. 11 Schematic illustration of the formation of RV/CAT-BP@MFL and its application for photothermally contrived drug delivery and oxygen self-enriched photodynamic multifarious cancer therapy. Reproduced from Ref. [94]

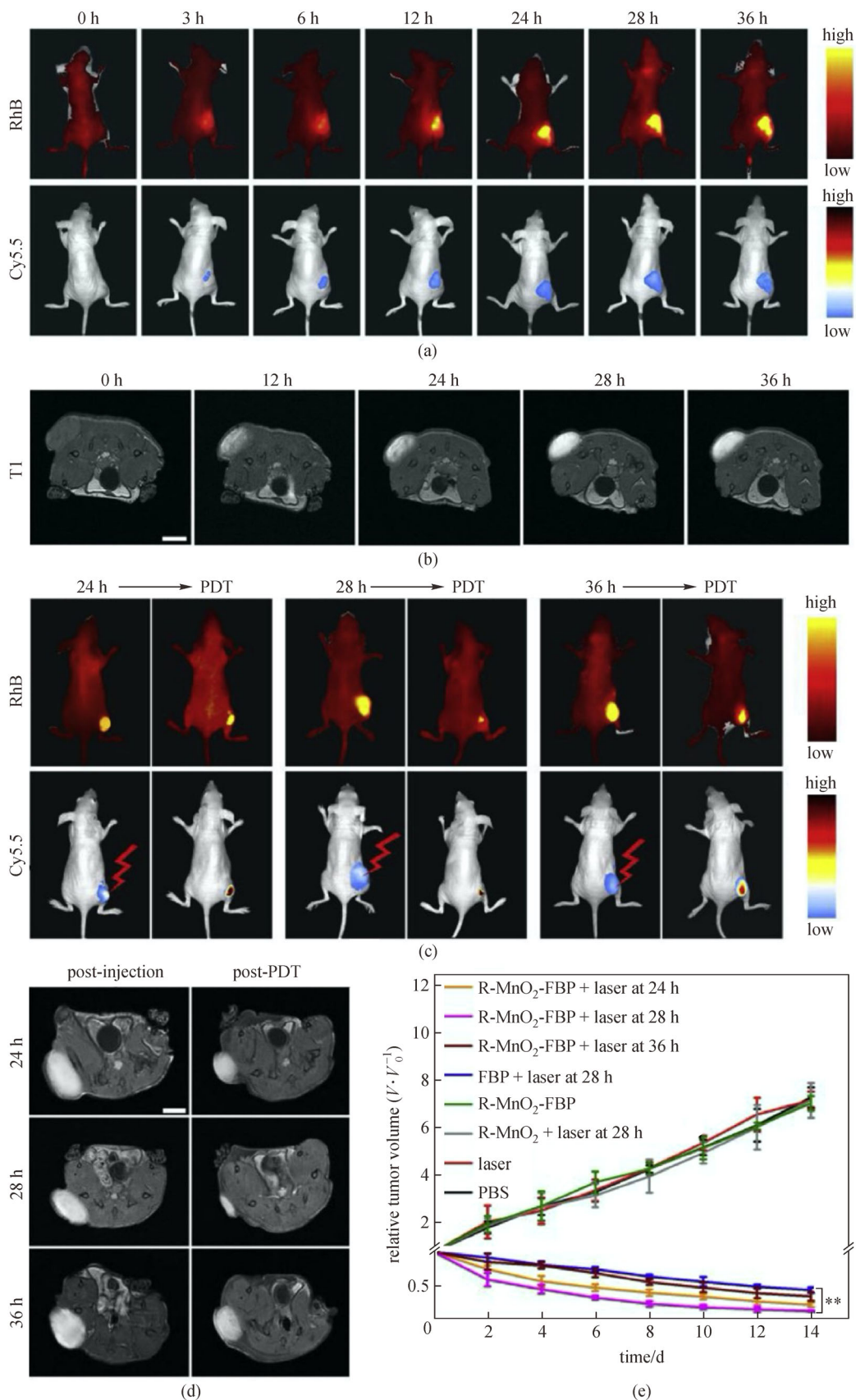


Fig. 12 (a) and (b) *In vivo* time-dependent imaging. (a) Time-dependent *in vivo* fluorescence images by dual-channel of RhB and Cy5.5. (b) MR images of a mouse bearing a subcutaneous HeLa tumor after being injected with R-MnO₂-FBP. Scale bar: 5.0 mm. (c)–(e) *In vivo* assessment of the PDT therapeutic efficacy as monitored by (c) fluorescence and (d) MRI on the tumor-bearing mice at 24, 28, and 36 h, separately, after injection of R-MnO₂-FBP. The tumors were irradiated by a 660-nm laser at 150 mW/cm² for 10 min. Scale bar: 5.0 mm. (e) Relative change of the averaged tumor volume after different treatments. Mean \pm SD, $n = 5$ (** $P < 0.01$). Reproduced from Ref. [96]

accuracy of the optimal duration, they exposed the mice to laser for different post-injection durations (24, 28, and 36 h) and subsequently compared the therapeutic efficacies. Dual-mode imaging shows that the fluorescence/MR signal intensity of the tumor site in the mice subjected to laser treatment for 28 h was much weaker than those in the 24- and 36-h groups, and the tumors in the 28-h group almost completely disappeared and were 10% smaller than those in the 24- and 36-h groups, indicating the maximal PDT efficiency (Figs. 12(c)–12(e)).

3.6 Functional layered-BP nanoparticles for other disease applications

3.6.1 Functional layered-BP nanoparticles for bone recovery

Because of the tough binding capability of P with metal ions, BPNSs have the potential to be potent nanocaptors for some physiologic diseases related to metal ions, such as Cu^{2+} , Ca^{2+} , Fe^{3+} , and Mg^{2+} . BPNSs have preeminent bioactivity; they can induce osteogenic differentiation in stem cells and arrest Ca^{2+} to spur biomineralization, which make them suitable for bone recovery applications [118,119]. The excellent osteoinduction capability of BP was regulated by an *in situ* P-driven Ca^{2+} mineralized extracellular matrix during BP degradation. BPNSs can promote bone regeneration and inhibit the progression of osteosarcoma *in vitro* through cancer-related inflammation inhibition [120,121]. For example, Wang et al. used inorganic BP nanocrystallites, decorated gelatin and polysaccharides, and mineralized CaP nanocrystallites to produce a double-network nanohydrogel for bone regeneration [97]. This crosslinked network could facilitate CaP complex formation and provide a favorable platform that mimics the microenvironment of extracellular matrices and enhances the activity of osteoblastic cell and bone generation physically and chemically. In addition, BPNSs, chitosan, and platelet-rich plasma are used in the synergistic treatment of rheumatoid arthritis (RA). BPNSs can help remove hyperplastic synoviocyte, which is the main characteristic of RA [98].

3.6.2 Functional layered-BP nanoparticles for brain disease

As a conductive material, BP has significant electrical conductivity due to its band dispersion, which can promote neural or cardiac regeneration by restoring the damaged electrical functions of impaired cardiomyocytes or neurons. Layered BP could intensify the differentiation of mesenchymal stem cells into neural-like cells under the electrical stimulation, showing application potentials for the design of biomaterials for electroactive tissues [99]. Qian et al. designed a nano-scaffold by the concentrically integrative bio-assembly of BP, which can restore

angiogenesis, neurogenesis, and immune homeostasis [122]. This layered-BP-based scaffold can stimulate Ca^{2+} -dependent axon regeneration and remyelination under slight oxidative stress; the researchers, in their demonstration, successfully regenerated a 20-mm peripheral nerve injury using the layered-BP-based scaffold. Conversely, it has also been demonstrated that layered BP can capture and regulate the concentration of Cu^{2+} , which can catalyze the production of cytotoxic ROS and, thenceforth, induce apoptosis of neuronal cells [100]. In neurodegenerative disease treatment, BP shows enhanced blood–brain barrier (BBB) permeability (21% in the *in vitro* model), and it can act as an antioxidant to decrease cellular ROS and protect cells from Cu^{2+} dyshomeostasis-related toxicity. Quite recently, Yang et al. successfully applied layered BP to Alzheimer's disease, a progressive and irreversible neurodegenerative disease [101]. One of the most important pathological features of Alzheimer's disease is cerebral plaques full of β -amyloid peptide ($\text{A}\beta$) [123]. A promising therapeutic strategy involves suppressing the aggregation of $\text{A}\beta$ monomers into cytotoxic β -sheet-rich amyloid fibers. On the basis of the $\text{A}\beta$ fibrillogenesis inhibition therapeutic proposal, they designed a series of peptide inhibitors, including LVFFARK (LK7), and utilized Cu^{2+} chelate and BBB-permeable layered BP to prevent the self-aggregation of LK7. Reciprocally, LK7 can prevent the oxidation of layered BP, thus stabilizing the nanomaterial (PEG-LK7@BP). ThT fluorescence assays showed an 83% decline in the $\text{A}\beta_{42}$ content (one of the most prevalent variations of $\text{A}\beta$) incubated with 100 $\mu\text{g}/\text{mL}$ PEG-LK7@BP, and atomic force microscope images revealed that the fibrils reduced notably in length and amount. All these results confirmed that PEG-LK7@BP dose-dependently restrains $\text{A}\beta_{42}$ fibrillization.

3.6.3 Functional layered-BP nanoparticles for progressive oxidative diseases

As discussed in the PDT-related section, excess ROS is cytotoxic, and it also causes progressive oxidative damage to cellular DNA of normal tissues and eventually cell death. The imbalance of ROS can activate the pathway of lysosomal injury, apoptosis, and necrosis. It has been reported that a variety of diseases (such as acute kidney injury, sepsis, stroke, and Parkinson's disease) are associated with excess ROS. Therefore, consuming ROS is a potential strategy for the treatment of progressive oxidative diseases. As an innate antioxidant, layered BP has the potential to treat progressive oxidative diseases. For example, in the treatment of acute kidney injuries, Hou et al. prepared a BP-related platform, taking advantage of its easy oxidation characteristic to ensure its combination with excessive ROS. Apart from being a nontoxic oxidative protector, the layered-BP direct kidney therapy

could facilitate kidney accumulation due to the flake-like morphology of layered BP [102].

4 Conclusion and prospects

Scientists have developed many new methods for the diagnosis and treatment of diseases, which depend on advanced instruments and nanomaterials with different structures and properties. With the rapid nanotechnological development and the special role of P in the human body, many inventions of layered-BP-based nanomaterials have been successfully applied in biomedicine. This paper classifies layered-BP-based nanomaterials according to their application in disease treatment and systematically reviews their research progress in areas of synthesis, corresponding properties, and biomedical applications in optical imaging, phototherapy, and delivery of biomolecules such as DNA, siRNA, and drugs. However, for further application of the layered-BP-based platform in biomedicine, several limitations must be overcome. First, the production of a large-scale layered-BP in uniform size is still challenging. Therefore, it is imperative to develop a more effective method for the mass production of layered BP. Second, functional modification is limited because of the lack of chemical groups. Controllable surface modification is difficult to achieve because of routine electrostatic interaction. Moreover, vdWs and covalent interactions could also be involved. We should design the protocol according to the desired functionalization to obtain a stable and effective agent. Third, hybrid BP platforms may possess significant potential for biomedical applications; however, they have been rarely studied. By combining BP with metals and nonmetals, enhanced stability and some synergistic properties for particular applications may be achieved. Fourth, the application of BP in bone recovery and other diseases (e.g., sepsis and stroke) has been less reported, even though it also has considerable potential; in this regard, an intensive investigation is required. Fifth, the biodegradation mechanism and *in vivo* long-term safety evaluation of BP remain unclear. More imaging models are required to explore the biological distribution and metabolic mechanism of BP action, and more tests are required to verify its safety *in vivo*. Layered-BP-based platforms have been applied to MRI, NIR-II imaging, and other imaging modalities, whereas only a few studies focus on PAI, which is expected to be a promising imaging method that can meet the requirements of high resolution and penetration depth simultaneously. In particular, the excellent photothermal conversion properties and NIR absorption spectra make layered BP a natural choice for PAI. Further, BP can easily be degraded *in vivo*, and the products are nontoxic and easily discharged out of the body, which lays the foundation for its applications *in vivo*. In addition, its high drug-loading rate and modifiable

properties extend its applicability in the treatment of diseases. By reviewing the development and application progress thus far, it is believed that with the rising interest in 2D materials, the layered-BP-based nanometer platform will play an important role in biomedical diagnosis and treatment.

Acknowledgements This work was supported in part by the National Natural Science Foundation of China (NSFC) (Grant Nos. 81930048, 81627805, and 81671726), Guangdong Science and Technology Commission (Nos. 2019BT02X105, 2019A1515011374), Hong Kong Research Grant Council (Nos. 25204416, R5029-19), Hong Kong Innovation and Technology Commission (Nos. ITS/022/18, GHP/043/19SZ, GHP/044/19GD), Shenzhen Science and Technology Innovation Commission (No. JCYJ20170818104421564), Guangdong Basic and Applied Basic Research Foundation for Distinguished Young Scholars (No. 2020B1515020027), and Guangzhou Science and Technology Bureau (No. 202002020070).

References

1. Shi Y, Liang X, Yuan B, Chen V, Li H, Hui F, Yu Z, Yuan F, Pop E, Wong H S P, Lanza M. Electronic synapses made of layered two-dimensional materials. *Nature Electronics*, 2018, 1(8): 458–465
2. Koppens F H, Mueller T, Avouris P, Ferrari A C, Vitiello M S, Polini M. Photodetectors based on graphene, other two-dimensional materials and hybrid systems. *Nature Nanotechnology*, 2014, 9(10): 780–793
3. Kang K, Lee K H, Han Y, Gao H, Xie S, Muller D A, Park J. Layer-by-layer assembly of two-dimensional materials into wafer-scale heterostructures. *Nature*, 2017, 550(7675): 229–233
4. Deng D, Novoselov K S, Fu Q, Zheng N, Tian Z, Bao X. Catalysis with two-dimensional materials and their heterostructures. *Nature Nanotechnology*, 2016, 11(3): 218–230
5. Jin L, Zhou J, Lai P. Tunable absorption characteristics in multilayered structures with graphene for biosensing. *Journal of Innovative Optical Health Sciences*, 2020, 13(04): 2050017
6. Zhang Y, Tang T T, Girit C, Hao Z, Martin M C, Zettl A, Crommie M F, Shen Y R, Wang F. Direct observation of a widely tunable bandgap in bilayer graphene. *Nature*, 2009, 459(7248): 820–823
7. Radovic L R, Bockrath B. On the chemical nature of graphene edges: origin of stability and potential for magnetism in carbon materials. *Journal of the American Chemical Society*, 2005, 127(16): 5917–5927
8. Tassin P, Koschny T, Soukoulis C M. Graphene for terahertz applications. *Science*, 2013, 341(6146): 620–621
9. Yang K, Feng L, Liu Z. Stimuli responsive drug delivery systems based on nano-graphene for cancer therapy. *Advanced Drug Delivery Reviews*, 2016, 105(Pt B): 228–241
10. Vogt P, De Padova P, Quaresima C, Avila J, Frantzeskakis E, Asensio M C, Resta A, Ealet B, Le Lay G. Silicene: compelling experimental evidence for graphenelike two-dimensional silicon. *Physical Review Letters*, 2012, 108(15): 155501
11. Seyler K L, Rivera P, Yu H, Wilson N P, Ray E L, Mandrus D G, Yan J, Yao W, Xu X. Signatures of moiré-trapped valley excitons in MoSe₂/WSe₂ heterobilayers. *Nature*, 2019, 567(7746): 66–70
12. Radisavljevic B, Radenovic A, Brivio J, Giacometti V, Kis A.

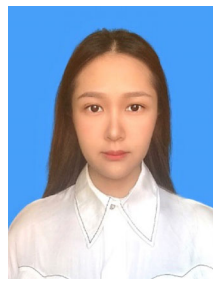
- Single-layer MoS₂ transistors. *Nature Nanotechnology*, 2011, 6(3): 147–150
13. Coleman J N, Lotya M, O'Neill A, Bergin S D, King P J, Khan U, Young K, Gaucher A, De S, Smith R J, Shvets I V, Arora S K, Stanton G, Kim H Y, Lee K, Kim G T, Duesberg G S, Hallam T, Boland J J, Wang J J, Donegan J F, Grunlan J C, Moriarty G, Shmeliov A, Nicholls R J, Perkins J M, Grievson E M, Theuwissen K, McComb D W, Nellist P D, Nicolosi V. Two-dimensional nanosheets produced by liquid exfoliation of layered materials. *Science*, 2011, 331(6017): 568–571
 14. Ge X, Xia Z, Guo S. Recent advances on black phosphorus for biomedicine and biosensing. *Advanced Functional Materials*, 2019, 29(29): 1900318
 15. An D, Fu J, Xie Z, Xing C, Zhang B, Wang B, Qiu M. Progress in the therapeutic applications of polymer-decorated black phosphorus and black phosphorus analog nanomaterials in biomedicine. *Journal of Materials Chemistry. B, Materials for Biology and Medicine*, 2020, 8(32): 7076–7120
 16. Qiu M, Ren W X, Jeong T, Won M, Park G Y, Sang D K, Liu L P, Zhang H, Kim J S. Omnipotent phosphorene: a next-generation, two-dimensional nanoplatform for multidisciplinary biomedical applications. *Chemical Society Reviews*, 2018, 47(15): 5588–5601
 17. You H, Jia Y, Wu Z, Wang F, Huang H, Wang Y. Room-temperature pyro-catalytic hydrogen generation of 2D few-layer black phosphorene under cold-hot alternation. *Nature Communications*, 2018, 9(1): 2889
 18. Lei W, Liu G, Zhang J, Liu M. Black phosphorus nanostructures: recent advances in hybridization, doping and functionalization. *Chemical Society Reviews*, 2017, 46(12): 3492–3509
 19. Castellanos-Gomez A, Vicarelli L, Prada E, Island J O, Narasimha-Acharya K L, Blanter S I, Groenendijk D J, Buscema M, Steele G A, Alvarez J V, Zandbergen H W, Palacios J J, van der Zant H S J. Isolation and characterization of few-layer black phosphorus. *2D Materials*, 2014, 1(2): 025001
 20. Xiong S, Chen X, Liu Y, Fan T, Wang Q, Zhang H, Chen T. Black phosphorus as a versatile nanoplatform: from unique properties to biomedical applications. *Journal of Innovative Optical Health Sciences*, 2020, 13(5): 2030008
 21. Abellán G, Lloret V, Mundloch U, Marcia M, Neiss C, Görling A, Varela M, Hauke F, Hirsch A. Noncovalent functionalization of black phosphorus. *Angewandte Chemie International Edition in English*, 2016, 55(47): 14557–14562
 22. Bolognesi M, Moschetto S, Trapani M, Prescimone F, Ferroni C, Manca G, Ienco A, Borsacchi S, Caporali M, Muccini M, Peruzzini M, Serrano-Ruiz M, Calucci L, Castriciano M A, Toffanin S. Noncovalent functionalization of 2D black phosphorus with fluorescent boronic derivatives of pyrene for probing and modulating the interaction with molecular oxygen. *ACS Applied Materials & Interfaces*, 2019, 11(25): 22637–22647
 23. Feng Q, Liu H, Zhu M, Shang J, Liu D, Cui X, Shen D, Kou L, Mao D, Zheng J, Li C, Zhang J, Xu H, Zhao J. Electrostatic functionalization and passivation of water-exfoliated few-layer black phosphorus by poly dimethyldiallyl ammonium chloride and its ultrafast laser application. *ACS Applied Materials & Interfaces*, 2018, 10(11): 9679–9687
 24. Zhang L, Gao L F, Li L, Hu C X, Yang Q Q, Zhu Z Y, Peng R, Wang Q, Peng Y, Jin J, Zhang H L. Negatively charged 2D black phosphorus for highly efficient covalent functionalization. *Materials Chemistry Frontiers*, 2018, 2(9): 1700–1706
 25. Meng Z, Stolz R M, Mendecki L, Mirica K A. Electrically-transduced chemical sensors based on two-dimensional nanomaterials. *Chemical Reviews*, 2019, 119(1): 478–598
 26. Jiang X, Jin H, Sun Y, Sun Z, Gui R. Assembly of black phosphorus quantum dots-doped MOF and silver nanoclusters as a versatile enzyme-catalyzed biosensor for solution, flexible substrate and latent fingerprint visual detection of baicalin. *Biosensors & Bioelectronics*, 2020, 152: 112012
 27. Irshad R, Tahir K, Li B, Sher Z, Ali J, Nazir S. A revival of 2D materials, phosphorene: its application as sensors. *Journal of Industrial and Engineering Chemistry*, 2018, 64: 6460–6469
 28. Xu Z, Hu L, Yuan J, Zhang Y, Guo Y, Jin Z, Long F, Long Y, Liang H, Ruan S, Zeng Y J. A fluorescence probe for metal ions based on black phosphorus quantum dots. *Advanced Materials Interfaces*, 2020, 7(7): 1902075
 29. Sun Y, Jin H, Jiang X, Gui R. Black phosphorus nanosheets adhering to thionine-doped 2D MOF as a smart aptasensor enabling accurate capture and ratiometric electrochemical detection of target microRNA. *Sensors and Actuators. B, Chemical*, 2020, 309: 127777
 30. Sun Z, Zhao Y, Li Z, Cui H, Zhou Y, Li W, Tao W, Zhang H, Wang H, Chu P K, Yu X F. TiL₄-coordinated black phosphorus quantum dots as an efficient contrast agent for *in vivo* photoacoustic imaging of cancer. *Small*, 2017, 13(11): 1602896
 31. Sun C, Wen L, Zeng J, Wang Y, Sun Q, Deng L, Zhao C, Li Z. One-pot solventless preparation of PEGylated black phosphorus nanoparticles for photoacoustic imaging and photothermal therapy of cancer. *Biomaterials*, 2016, 91: 81–89
 32. Tao W, Zhu X, Yu X, Zeng X, Xiao Q, Zhang X, Ji X, Wang X, Shi J, Zhang H, Mei L. Black phosphorus nanosheets as a robust delivery platform for cancer theranostics. *Advanced Materials*, 2017, 29(1): 1603276
 33. Wang H, Yang X, Shao W, Chen S, Xie J, Zhang X, Wang J, Xie Y. Ultrathin black phosphorus nanosheets for efficient singlet oxygen generation. *Journal of the American Chemical Society*, 2015, 137(35): 11376–11382
 34. Qian X, Gu Z, Chen Y. Two-dimensional black phosphorus nanosheets for theranostic nanomedicine. *Materials Horizons*, 2017, 4(5): 800–816
 35. Choi J R, Yong K W, Choi J Y, Nilghaz A, Lin Y, Xu J, Lu X. Black phosphorus and its biomedical applications. *Theranostics*, 2018, 8(4): 1005–1026
 36. Childers D L, Corman J, Edwards M, Elser J J. Sustainability challenges of phosphorus and food: solutions from closing the human phosphorus cycle. *Bioscience*, 2011, 61(2): 117–124
 37. Qiu M, Singh A, Wang D, Qu J, Swihart M, Zhang H, Prasad P N. Biocompatible and biodegradable inorganic nanostructures for nanomedicine: silicon and black phosphorus. *Nano Today*, 2019, 25: 135–155
 38. Wang Z, Liu Z, Su C, Yang B, Fei X, Li Y, Hou Y, Zhao H, Guo Y, Zhuang Z, Zhong H, Guo Z. Biodegradable black phosphorus-based nanomaterials in biomedicine: theranostic applications. *Current Medicinal Chemistry*, 2019, 26(10): 1788–1805

39. Anju S, Ashtami J, Mohanan P V. Black phosphorus, a prospective graphene substitute for biomedical applications. *Materials Science and Engineering C*, 2019, 97: 978–993
40. Yu J, Wang Q, O'Hare D, Sun L. Preparation of two dimensional layered double hydroxide nanosheets and their applications. *Chemical Society Reviews*, 2017, 46(19): 5950–5974
41. López-Cabrelles J, Mañas-Valero S, Vitórica-Yrezábal I J, Bereciartua P J, Rodríguez-Velamazán J A, Waerenborgh J C, Vieira B J C, Davidovikj D, Steeneken P G, van der Zant H S J, Mínguez Espallargas G, Coronado E. Isorecticular two-dimensional magnetic coordination polymers prepared through pre-synthetic ligand functionalization. *Nature Chemistry*, 2018, 10(10): 1001–1007
42. Han J H, Kwak M, Kim Y, Cheon J. Recent advances in the solution-based preparation of two-dimensional layered transition metal chalcogenide nanostructures. *Chemical Reviews*, 2018, 118(13): 6151–6188
43. Eswaraiyah V, Zeng Q, Long Y, Liu Z. Black phosphorus nanosheets: synthesis, characterization and applications. *Small*, 2016, 12(26): 3480–3502
44. Bridgman P W. Two new modifications of phosphorus. *Journal of the American Chemical Society*, 1914, 36(7): 1344–1363
45. Aldave S H, Yogeesh M N, Zhu W, Kim J, Sonde S S, Nayak A P, Akinwande D. Characterization and sonochemical synthesis of black phosphorus from red phosphorus. *2D Materials*, 2016, 3(1): 014007
46. Endo S, Akahama Y, Terada S, Narita S. Growth of large single crystals of black phosphorus under high pressure. *Japanese Journal of Applied Physics*, 1982, 21(Part 2, No. 8): L482–L484
47. Krebs H, Weitz H, Worms K H. About the structure and properties of semimetals VIII. The catalytic representation of black phosphorus. *Zeitschrift für Anorganische und Allgemeine Chemie*, 1955, 280(1–3): 119–133
48. Baba M, Izumida F, Takeda Y, Morita A. Preparation of black phosphorus single crystals by a completely closed bismuth-flux method and their crystal morphology. *Japanese Journal of Applied Physics*, 1989, 28(Part 1, No. 6): 1019–1022
49. Lange S, Schmidt P, Au Nilges T. 3SnP₇@black phosphorus: an easy access to black phosphorus. *Inorganic Chemistry*, 2007, 46(10): 4028–4035
50. Köpf M, Eckstein N, Pfister D, Grotz C, Krüger I, Greiwe M, Hansen T, Kohlmann H, Nilges T. Access and *in situ* growth of phosphorene-precursor black phosphorus. *Journal of Crystal Growth*, 2014, 405: 6–10
51. Sun Q, Zhao X, Feng Y, Wu Y, Zhang Z, Zhang X, Wang X, Feng S, Liu X. Pressure quenching: a new route for the synthesis of black phosphorus. *Inorganic Chemistry Frontiers*, 2018, 5(3): 669–674
52. Wang D, Yi P, Wang L, Zhang L, Li H, Lu M, Xie X, Huang L, Huang W. Revisiting the growth of black phosphorus in Sn-I assisted reactions. *Frontiers in Chemistry*, 2019, 7: 21
53. Novoselov K S, Jiang D, Schedin F, Booth T J, Khotkevich V V, Morozov S V, Geim A K. Two-dimensional atomic crystals. *Proceedings of the National Academy of Sciences of the United States of America*, 2005, 102(30): 10451–10453
54. Hultgren R, Gingrich N S, Warren B E. The atomic distribution in red and black phosphorus and the crystal structure of black phosphorus. *Journal of Chemical Physics*, 1935, 3(6): 351–355
55. Liu F, Wu W, Bai Y, Chae S H, Li Q, Wang J, Hone J, Zhu X Y. Disassembling 2D van der Waals crystals into macroscopic monolayers and reassembling into artificial lattices. *Science*, 2020, 367(6480): 903–906
56. Kou L, Chen C, Smith S C. Phosphorene: fabrication, properties, and applications. *Journal of Physical Chemistry Letters*, 2015, 6(14): 2794–2805
57. Huang Y, Sutter E, Shi N N, Zheng J, Yang T, Englund D, Gao H J, Sutter P. Reliable exfoliation of large-area high-quality flakes of graphene and other two-dimensional materials. *ACS Nano*, 2015, 9(11): 10612–10620
58. Cai X, Luo Y, Liu B, Cheng H M. Preparation of 2D material dispersions and their applications. *Chemical Society Reviews*, 2018, 47(16): 6224–6266
59. Guan L, Xing B, Niu X, Wang D, Yu Y, Zhang S, Yan X, Wang Y, Sha J. Metal-assisted exfoliation of few-layer black phosphorus with high yield. *Chemical Communications (Cambridge)*, 2018, 54(6): 595–598
60. Lu W, Nan H, Hong J, Chen Y, Zhu C, Liang Z, Ma X, Ni Z, Jin C, Zhang Z. Plasma-assisted fabrication of monolayer phosphorene and its Raman characterization. *Nano Research*, 2014, 7(6): 853–859
61. Pei J, Gai X, Yang J, Wang X, Yu Z, Choi D Y, Luther-Davies B, Lu Y. Producing air-stable monolayers of phosphorene and their defect engineering. *Nature Communications*, 2016, 7(1): 10450
62. Hanlon D, Backes C, Doherty E, Cucinotta C S, Berner N C, Boland C, Lee K, Harvey A, Lynch P, Gholamvand Z, Zhang S, Wang K, Moynihan G, Pokle A, Ramasse Q M, McEvoy N, Blau W J, Wang J, Abellan G, Hauke F, Hirsch A, Sanvito S, O'Regan D D, Duesberg G S, Nicolosi V, Coleman J N. Liquid exfoliation of solvent-stabilized few-layer black phosphorus for applications beyond electronics. *Nature Communications*, 2015, 6(1): 8563
63. Kang J, Wells S A, Wood J D, Lee J H, Liu X, Ryder C R, Zhu J, Guest J R, Husko C A, Hersam M C. Stable aqueous dispersions of optically and electronically active phosphorene. *Proceedings of the National Academy of Sciences of the United States of America*, 2016, 113(42): 11688–11693
64. Brent J R, Savjani N, Lewis E A, Haigh S J, Lewis D J, O'Brien P. Production of few-layer phosphorene by liquid exfoliation of black phosphorus. *Chemical Communications (Cambridge)*, 2014, 50(87): 13338–13341
65. Lin S, Chui Y, Li Y, Lau S P. Liquid-phase exfoliation of black phosphorus and its applications. *FlatChem*, 2017, 2: 15–37
66. Yasaei P, Kumar B, Foroozan T, Wang C, Asadi M, Tuschel D, Indacochea J E, Klie R F, Salehi-Khojin A. High-quality black phosphorus atomic layers by liquid-phase exfoliation. *Advanced Materials*, 2015, 27(11): 1887–1892
67. Woomer A H, Farnsworth T W, Hu J, Wells R A, Donley C L, Warren S C. Phosphorene: synthesis, scale-up, and quantitative optical spectroscopy. *ACS Nano*, 2015, 9(9): 8869–8884
68. Chu P. Plasma-surface modification of biomaterials. *Materials Science and Engineering R Reports*, 2002, 36(5–6): 143–206
69. Liu R, Wang Y, Liu D, Zou Y, Wang S. Water-plasma-enabled exfoliation of ultrathin layered double hydroxide nanosheets with

- multivacancies for water oxidation. *Advanced Materials*, 2017, 29 (30): 1701546
70. Lee H, Bratescu M A, Ueno T, Saito N. Solution plasma exfoliation of graphene flakes from graphite electrodes. *RSC Advances*, 2014, 4(93): 51758–51765
71. Elumalai S, Su C Y, Yoshimura M. Scalable one-pot synthesis of nitrogen and boron co-doped few layered graphene by submerged liquid plasma exfoliation. *Frontiers in Materials*, 2019, 6: 216
72. Huang H, Gao M, Kang Y, Li J, Wang J, Wu L, Chu P K, Huang Y, Ibarra M R, Yu X F. Rapid and scalable production of high-quality phosphorene by plasma-liquid technology. *Chemical Communications (Cambridge)*, 2020, 56(2): 221–224
73. Hernandez Y, Nicolosi V, Lotya M, Blighe F M, Sun Z, De S, McGovern I T, Holland B, Byrne M, Gun'Ko Y K, Boland J J, Niraj P, Duesberg G, Krishnamurthy S, Goodhue R, Hutchison J, Scardaci V, Ferrari A C, Coleman J N. High-yield production of graphene by liquid-phase exfoliation of graphite. *Nature Nanotechnology*, 2008, 3(9): 563–568
74. Li X, Cai W, An J, Kim S, Nah J, Yang D, Piner R, Velamakanni A, Jung I, Tutuc E, Banerjee S K, Colombo L, Ruoff R S. Large-area synthesis of high-quality and uniform graphene films on copper foils. *Science*, 2009, 324(5932): 1312–1314
75. Kim K S, Zhao Y, Jang H, Lee S Y, Kim J M, Kim K S, Ahn J H, Kim P, Choi J Y, Hong B H. Large-scale pattern growth of graphene films for stretchable transparent electrodes. *Nature*, 2009, 457(7230): 706–710
76. Li X, Deng B, Wang X, Chen S, Vaisman M, Karato S, Pan G, Lee L M, Cha J, Wang H, Xia F. Synthesis of thin-film black phosphorus on a flexible substrate. *2D Materials*, 2015, 2(3): 031002
77. Smith J B, Hagaman D, Ji H F. Growth of 2D black phosphorus film from chemical vapor deposition. *Nanotechnology*, 2016, 27 (21): 215602
78. Li C, Wu Y, Deng B, Xie Y, Guo Q, Yuan S, Chen X, Bhuiyan M, Wu Z, Watanabe K, Taniguchi T, Wang H, Cha J J, Snure M, Fei Y, Xia F. Synthesis of crystalline black phosphorus thin film on sapphire. *Advanced Materials*, 2018, 30(6): 1703748
79. Deng L, Xu Y, Sun C, Yun B, Sun Q, Zhao C, Li Z. Functionalization of small black phosphorus nanoparticles for targeted imaging and photothermal therapy of cancer. *Science Bulletin*, 2018, 63(14): 917–924
80. Xu Y, Ren F, Liu H, Zhang H, Han Y, Liu Z, Wang W, Sun Q, Zhao C, Li Z. Cholesterol-modified black phosphorus nanospheres for the first NIR-II fluorescence bioimaging. *ACS Applied Materials & Interfaces*, 2019, 11(24): 21399–21407
81. Guo T, Lin Y, Jin G, Weng R, Song J, Liu X, Huang G, Hou L, Yang H. Manganese-phenolic network-coated black phosphorus nanosheets for theranostics combining magnetic resonance/photoacoustic dual-modal imaging and photothermal therapy. *Chemical Communications (Cambridge)*, 2019, 55(6): 850–853
82. Zhang Q, Wang W, Zhang M, Wu F, Zheng T, Sheng B, Liu Y, Shen J, Zhou N, Sun Y. A theranostic nanocomposite with integrated black phosphorus nanosheet, Fe₃O₄@MnO₂-doped upconversion nanoparticles and chlorin for simultaneous multimodal imaging, highly efficient photodynamic and photothermal therapy. *Chemical Engineering Journal*, 2020, 391: 123525
83. Zhao Y, Tong L, Li Z, Yang N, Fu H, Wu L, Cui H, Zhou W, Wang J, Wang H, Chu P K, Yu X F. Stable and multifunctional dye-modified black phosphorus nanosheets for near-infrared imaging-guided photothermal therapy. *Chemistry of Materials*, 2017, 29 (17): 7131–7139
84. Geng B, Shen W, Li P, Fang F, Qin H, Li X K, Pan D, Shen L. Carbon dot-passivated black phosphorus nanosheet hybrids for synergistic cancer therapy in the NIR-II window. *ACS Applied Materials & Interfaces*, 2019, 11(48): 44949–44960
85. Huang W Q, Wang F, Nie X, Zhang Z, Chen G, Xia L, Wang L H, Ding S G, Hao Z Y, Zhang W J, Hong C Y, You Y Z. Stable black phosphorus nanosheets exhibiting high tumor-accumulating and mitochondria-targeting for efficient photothermal therapy via double functionalization. *ACS Applied Bio Materials*, 2020, 3 (2): 1176–1186
86. Chen B Q, Kankala R K, Zhang Y, Xiang S T, Tang H X, Wang Q, Yang D Y, Wang S B, Zhang Y S, Liu G, Chen A Z. Gambogic acid augments black phosphorus quantum dots (BPQDs)-based synergistic chemo-photothermal therapy through downregulating heat shock protein expression. *Chemical Engineering Journal*, 2020, 390: 124312
87. Guo T, Wu Y, Lin Y, Xu X, Lian H, Huang G, Liu J Z, Wu X, Yang H H. Black phosphorus quantum dots with renal clearance property for efficient photodynamic therapy. *Small*, 2018, 14(4): 1702815
88. Liu J, Du P, Mao H, Zhang L, Ju H, Lei J. Dual-triggered oxygen self-supply black phosphorus nanosystem for enhanced photodynamic therapy. *Biomaterials*, 2018, 172: 83–91
89. Chen W, Ouyang J, Liu H, Chen M, Zeng K, Sheng J, Liu Z, Han Y, Wang L, Li J, Deng L, Liu Y N, Guo S. Black phosphorus nanosheet-based drug delivery system for synergistic photodynamic/photothermal/chemotherapy of cancer. *Advanced Materials*, 2017, 29(5): 1603864
90. Qiu M, Wang D, Liang W, Liu L, Zhang Y, Chen X, Sang D K, Xing C, Li Z, Dong B, Xing F, Fan D, Bao S, Zhang H, Cao Y. Novel concept of the smart NIR-light-controlled drug release of black phosphorus nanostructure for cancer therapy. *Proceedings of the National Academy of Sciences of the United States of America*, 2018, 115(3): 501–506
91. Gao N, Nie J, Wang H, Xing C, Mei L, Xiong W, Zeng X, Peng Z. A versatile platform based on black phosphorus nanosheets with enhanced stability for cancer synergistic therapy. *Journal of Biomedical Nanotechnology*, 2018, 14(11): 1883–1897
92. Zeng X, Luo M, Liu G, Wang X, Tao W, Lin Y, Ji X, Nie L, Mei L. Polydopamine-modified black phosphorous nanocapsule with enhanced stability and photothermal performance for tumor multimodal treatments. *Advanced Science (Weinheim, Baden-Wuerttemberg, Germany)*, 2018, 5(10): 1800510
93. Chen L, Qian M, Jiang H, Zhou Y, Du Y, Yang Y, Huo T, Huang R, Wang Y. Multifunctional mesoporous black phosphorus-based nanosheet for enhanced tumor-targeted combined therapy with biodegradation-mediated metastasis inhibition. *Biomaterials*, 2020, 236: 119770
94. Hai L, Zhang A, Wu X, Cheng H, He D, Wang T, He X, Wang K. Liposome-stabilized black phosphorus for photothermal drug delivery and oxygen self-enriched photodynamic therapy. *ACS Applied Nano Materials*, 2020, 3(1): 563–575

95. Li Z, Hu Y, Fu Q, Liu Y, Wang J, Song J, Yang H. NIR/ROS-responsive black phosphorus QD vesicles as immunoadjuvant carrier for specific cancer photodynamic immunotherapy. *Advanced Functional Materials*, 2020, 30(3): 1905758
96. Liu J, Du P, Liu T, Córdova Wong B J, Wang W, Ju H, Lei J. A black phosphorus/manganese dioxide nanoplatform: oxygen self-supply monitoring, photodynamic therapy enhancement and feedback. *Biomaterials*, 2019, 192: 179–188
97. Wang Z, Zhao J, Tang W, Hu L, Chen X, Su Y, Zou C, Wang J, Lu W W, Zhen W, Zhang R, Yang D, Peng S. Multifunctional nanoengineered hydrogels consisting of black phosphorus nanosheets upregulate bone formation. *Small*, 2019, 15(41): 1901560
98. Pan W, Dai C, Li Y, Yin Y, Gong L, Machuki J O, Yang Y, Qiu S, Guo K, Gao F. PRP-chitosan thermoresponsive hydrogel combined with black phosphorus nanosheets as injectable biomaterial for biotherapy and phototherapy treatment of rheumatoid arthritis. *Biomaterials*, 2020, 239: 119851
99. Xu C, Xu Y, Yang M, Chang Y, Nie A, Liu Z, Wang J, Luo Z. Black-phosphorus-incorporated hydrogel as a conductive and biodegradable platform for enhancement of the neural differentiation of mesenchymal stem cells. *Advanced Functional Materials*, 2020, 30(39): 2000177
100. Chen W, Ouyang J, Yi X, Xu Y, Niu C, Zhang W, Wang L, Sheng J, Deng L, Liu Y N, Guo S. Black phosphorus nanosheets as a neuroprotective nanomedicine for neurodegenerative disorder therapy. *Advanced Materials*, 2018, 30(3): 1703458
101. Yang J, Liu W, Sun Y, Dong X. LVFFARK-PEG-stabilized black phosphorus nanosheets potently inhibit amyloid- β fibrillogenesis. *Langmuir*, 2020, 36(7): 1804–1812
102. Hou J, Wang H, Ge Z, Zuo T, Chen Q, Liu X, Mou S, Fan C, Xie Y, Wang L. Treating acute kidney injury with antioxidative black phosphorus nanosheets. *Nano Letters*, 2020, 20(2): 1447–1454
103. Huang X, Shang W, Deng H, Zhou Y, Cao F, Fang C, Lai P, Tian J. Clothing spiny nanoprobe against the mononuclear phagocyte system clearance *in vivo*: photoacoustic diagnosis and photothermal treatment of early stage liver cancer with erythrocyte membrane-camouflaged gold nanostars. *Applied Materials Today*, 2020, 18: 100484
104. Lai P, Wang L, Tay J W, Wang L V. Photoacoustically guided wavefront shaping for enhanced optical focusing in scattering media. *Nature Photonics*, 2015, 9(2): 126–132
105. Zhou Y, Cao F, Li H, Huang X, Wei D, Wang L, Lai P. Photoacoustic imaging of microenvironmental changes in facial cupping therapy. *Biomedical Optics Express*, 2020, 11(5): 2394–2401
106. Shao J, Xie H, Huang H, Li Z, Sun Z, Xu Y, Xiao Q, Yu X F, Zhao Y, Zhang H, Wang H, Chu P K. Biodegradable black phosphorus-based nanospheres for *in vivo* photothermal cancer therapy. *Nature Communications*, 2016, 7(1): 12967
107. Kenry Y, Duan Y, Liu B. Recent advances of optical imaging in the second near-infrared window. *Advanced Materials*, 2018, 30(47): 1802394
108. Gu C, Zheng C, Liu B, Feng T, Ma J, Sun H. Synthesis of a dithieno[3,2-b:2',3'-d]silole-based conjugated polymer and characterization of its short wave near-infrared fluorescence properties. *Journal of Innovative Optical Health Sciences*, 2020, 13(5): 2041002
109. Idris N M, Gnanasammandhan M K, Zhang J, Ho P C, Mahendran R, Zhang Y. *In vivo* photodynamic therapy using upconversion nanoparticles as remote-controlled nanotransducers. *Nature Medicine*, 2012, 18(10): 1580–1585
110. Hemmer E, Benayas A, Légaré F, Vetrone F. Exploiting the biological windows: current perspectives on fluorescent bioprobes emitting above 1000 nm. *Nanoscale Horizons*, 2016, 1(3): 168–184
111. Liu Y, Liu H, Yan H, Liu Y, Zhang J, Shan W, Lai P, Li H, Ren L, Li Z, Nie L. Aggregation-induced absorption enhancement for deep near-infrared II photoacoustic imaging of brain gliomas *in vivo*. *Advanced Science (Weinheim, Baden-Wuerttemberg, Germany)*, 2019, 6(8): 1801615
112. Brown S B, Brown E A, Walker I. The present and future role of photodynamic therapy in cancer treatment. *The Lancet. Oncology*, 2004, 5(8): 497–508
113. Castano A P, Mroz P, Hamblin M R. Photodynamic therapy and anti-tumour immunity. *Nature Reviews. Cancer*, 2006, 6(7): 535–545
114. Fu J, An D, Song Y, Wang C, Qiu M, Zhang H. Janus nanoparticles for cellular delivery chemotherapy: recent advances and challenges. *Coordination Chemistry Reviews*, 2020, 422: 213467
115. Devlin E J, Denson L A, Whitford H S. Cancer treatment side effects: a meta-analysis of the relationship between response expectancies and experience. *Journal of Pain and Symptom Management*, 2017, 54(2): 245–258
116. Rothenberg M, Ling V. Multidrug resistance: molecular biology and clinical relevance. *Journal of the National Cancer Institute*, 1989, 81(12): 907–910
117. Guo R, Peng H, Tian Y, Shen S, Yang W. Mitochondria-targeting magnetic composite nanoparticles for enhanced phototherapy of cancer. *Small*, 2016, 12(33): 4541–4552
118. Huang K, Wu J, Gu Z. Black phosphorus hydrogel scaffolds enhance bone regeneration via a sustained supply of calcium-free phosphorus. *ACS Applied Materials & Interfaces*, 2019, 11(3): 2908–2916
119. Wang Y, Hu X, Zhang L, Zhu C, Wang J, Li Y, Wang Y, Wang C, Zhang Y, Yuan Q. Bioinspired extracellular vesicles embedded with black phosphorus for molecular recognition-guided biomimetic mineralization. *Nature Communications*, 2019, 10(1): 2829
120. Raucchi M G, Fasolino I, Caporali M, Serrano-Ruiz M, Soriente A, Peruzzini M, Ambrosio L. Exfoliated black phosphorus promotes *in vitro* bone regeneration and suppresses osteosarcoma progression through cancer-related inflammation inhibition. *ACS Applied Materials & Interfaces*, 2019, 11(9): 9333–9342
121. Lee Y B, Song S J, Shin Y C, Jung Y J, Kim B, Kang M S, Kwon I K, Hyon S H, Lee H U, Jung S H, Lim D, Han D W. Ternary nanofiber matrices composed of PCL/black phosphorus/collagen to enhance osteodifferentiation. *Journal of Industrial and Engineering Chemistry*, 2019, 80: 802–810
122. Qian Y, Yuan W E, Cheng Y, Yang Y, Qu X, Fan C. Concentrically integrative bioassembly of a three-dimensional black phosphorus nanoscaffold for restoring neurogenesis, angiogenesis, and immune homeostasis. *Nano Letters*, 2019, 19(12): 8990–9001

123. Querfurth H W, LaFerla F M. Alzheimer's disease. *New England Journal of Medicine*, 2010, 362(4): 329–344



Xiazi Huang received her bachelor's degree in Pharmacy from Sun Yat-Sen University, China, in 2015 and M.Sc. degree in Biomedical Engineering from Hong Kong Polytechnic University, China, in 2016. After that, she joined a biophotonics laboratory at Hong Kong Polytechnic University, China, as a research assistant. She is currently a Ph.D. student at Department of Biomedical Engineering, Hong Kong Polytechnic University, China. Her research focuses on the design of nanoparticles for enhanced imaging diagnosis and cancer treatment.



Yingying ZHOU is a Ph.D. student at Department of Biomedical Engineering, Hong Kong Polytechnic University, China. She received her bachelor's degree from Sun Yat-Sen University, China. Her research focuses on photoacoustic microscopy and its applications.



Chi Man Woo received her M.Sc. degree in Biomedical Engineering from Hong Kong Polytechnic University, China, in 2019 and B.Eng. degree in Medical Engineering from The University of Hong Kong, China, in 2017. She is currently a research assistant in a biophotonics laboratory at Hong Kong Polytechnic University, China. Her research focuses on biomedical imaging and optical wavefront shaping for deep-tissue focusing.



Yue Pan received his B.Sc. degree in 2003, followed by a M.Sc. degree from University of Science and Technology of China (USTC), China, in 2006. He obtained his Ph.D. degree in 2012 from Brandeis University, USA, under the supervision of Prof. Bing Xu. Before starting his independent research at Soochow University, China, in 2013, he was a postdoctoral fellow at Harvard Medical School, USA. He is now a full professor at Sun Yat-Sen Memorial Hospital, Sun Yat-Sen University, China. He has published 32 papers as the corresponding author and 7 as the first author in several journals, including *Chemical Society Reviews*, *Journal of the American Chemical Society*, *Nano Energy*, and *Biosensors and Bioelectronics*. His research focuses on the biomedical applications of functionalized nanomaterials, which have been widely reported and cited by *Nature Materials*, *Nature Reviews Chemistry*, *Nature Protocols*, *Nature Biomedical Engineering*, etc. His research has also been highlighted by "Chemistry

World" of the Royal Society of Chemistry, "Advanced Science News", and "Chemistry Views" by Wiley and ranked by "Faculty of 1000" among the top 2% of published articles in biology and medicine. He was honored as one of the "Top 1% Most Cited Chinese Researchers" by the Royal Society of Chemistry and Distinguished Young Scholars by Guangdong Basic and Applied Basic Research Foundation.



Liming Nie earned his Ph.D. degree in Optics from South China Normal University, China. He received his postdoctoral training under Dr. Lihong V. Wang at Washington University in St. Louis, USA, from 2010 to 2012. Thereafter, he worked on molecular imaging as a research associate at National Institute of Health, USA. In 2014, he joined Xiamen University, China, as a faculty member and was promoted to full professor in 2018. His laboratory is transitioning to the Guangdong Academy of Medical Sciences, China. He edited and co-authored two textbooks on molecular imaging. His laboratory focuses on optical molecular imaging technology advancement and applications, mainly on photoacoustic microscopy, functional photoacoustic tomography, and other imaging modalities, such as magnetic resonance imaging and positron emission tomography. He has published over 70 peer-reviewed articles in several journals, including *Nature Communications*, *Angewandte Chemie International Edition*, *European Radiology*, and *The Journal of Nuclear Medicine*, and has delivered more than 30 plenary speeches or invited talks in international conferences. His work has been cited by *Nature Method*, *Neuron*, *PNAS*, etc. His Google Scholar H-index and citations have reached 34 and 4300, respectively. He has received numerous research funding awards from the National Natural Science Foundation of China as well as the Ministry of Science and Technology of China. He received the ACS Young Scientist Award and the first-place award of Huaxia Medical Technology.



Puxiang Lai received his bachelor's degree from Tsinghua University, China, in 2002, M.Sc. degree from Chinese Academy of Sciences, China, in 2005, and Ph.D. degree from Boston University, USA, in 2011. After that, he joined Dr. Lihong V. Wang's laboratory at Washington University in St. Louis, USA, as a Postdoctoral Research Associate. In September 2015, he joined Department of Biomedical Engineering at Hong Kong Polytechnic University, China, as a tenure-track assistant professor.

Dr. Lai's research focuses on the synergy of light and sound as well as their applications in biomedicine, such as wavefront shaping, photoacoustic imaging, acousto-optic imaging, and computational optical imaging. His research has fueled more than 50 publications in top journals, such as *Nature Photonics*, *Nature Communications*, and *Advanced Sciences*. Since 2015, his research has been continuously supported by the National Natural Science Foundation

of China (NSFC), Hong Kong Research Grant Council (RGC), Hong Kong Innovation and Technology Commission (ITC), Department of Science and Technology of Guangdong Province, and Shenzhen Science and Technology Innovation Commission (STIC), with an allocated budget of more than 19 million Hong Kong dollars.

Dr. Lai was awarded the 2016–2017 Hong Kong RGC Early Career Award, 2018 Hong Kong Polytechnic University Faculty of Engineering Research Grant Achievement Award, 2019 PolyU K.C. Wong Belt and Road Visiting Fellowship Award, and 2020 Hong

Kong Polytechnic University Faculty of Engineering Faculty Research Award. In recognition of his contribution to the field, currently, Puxiang serves as an Associate Editor of *Journal of Visual Computing for Industry, Biomedicine, and Art* (VCIBA); a Guest Editor of *Journal of Innovative Optics in Health and Science* (JIOHS); a Committee Member of the Biomedical Optics Panel in the Chinese Society of Biomedical Engineering; and a Member of the Medical Instrument Judging Panel in the Shenzhen Science and Technology Innovation Commission.